Physics and Control of Cavitation

Jean-Pierre FRANC
University of Grenoble
LEGI – BP 53 – 38041 Grenoble Cedex 9
FRANCE

Jean-Pierre.Franc@hmg.inpg.fr

ABSTRACT

The objective of the present chapter[1] is to provide the basic concepts and tools required to understand the inception and development of cavitation in liquid flows. The influence of various parameters as the boundary layer and nuclei content is discussed. A special attention is given to thermal effects which may significantly influence the development of cavitation in thermosensitive fluids as cryogenic liquids. The main types of cavitation (partial attached cavities, travelling bubble cavitation, vortex cavitation and shear cavitation) are presented.

NOMENCLATURE

B	factor of Stepanov (equation (29))
C_p	pressure coefficient (equation (3))
$c_{p\ell}$	heat capacity of the liquid
D	characteristic length scale (section 4.4)
F	function of radius defined in section 3.3.3
f	bubble resonance frequency (section 3.3.3)
h	heat transfer coefficient at interface (equation (37))
L	latent heat of vaporization
Nu	Nusselt number: $h\,D\,/\,\lambda_\ell$
p	pressure
p_g	non-condensable gas pressure
p_v	vapour pressure
R	bubble radius
$\overline{R}$	non dimensional radius $R\,/\,D$
$\dot{R}, \ddot{R}$	time derivatives of the bubble radius
r	distance from bubble center
S	surface tension
T	temperature
t	time
V, v	velocity
V_ℓ, V_v	volumes (section 4)

Greek Symbols

α_ℓ	liquid thermal diffusivity
γ	ratio of heat capacities of gas
Δp_v^*	vapour pressure drop (equation (34))
ΔT	temperature drop due to thermal effects
ΔT^*	reference temperature difference (equation (30))
λ_ℓ	liquid thermal conductivity
μ	dynamic viscosity of the liquid
ν	kinematic viscosity $\mu\,/\,\rho$ of the liquid
Π	non-dimensional pressure (equation (23))
ρ	liquid density
σ_v	cavitation parameter (equation (5))
τ	bubble collapse time (section 3.3.1) transit time (section 4.4)
τ_T	thermal time (equation (44))

[1] Two lectures, von Kàrmàn Institute Lecture Series "Design, Analysis and Experimental Investigation of High Speed Pumps".

Franc, J.-P. (2006) Physics and Control of Cavitation. In *Design and Analysis of High Speed Pumps* (pp. 2-1 – 2-36). Educational Notes RTO-EN-AVT-143, Paper 2. Neuilly-sur-Seine, France: RTO. Available from: http://www.rto.nato.int/abstracts.asp.

Report Documentation Page

Form Approved
OMB No. 0704-0188

1. REPORT DATE	2. REPORT TYPE	3. DATES COVERED
01 NOV 2006	**N/A**	**-**

4. TITLE AND SUBTITLE	5a. CONTRACT NUMBER
Physics and Control of Cavitation	5b. GRANT NUMBER
	5c. PROGRAM ELEMENT NUMBER
6. AUTHOR(S)	5d. PROJECT NUMBER
	5e. TASK NUMBER
	5f. WORK UNIT NUMBER
7. PERFORMING ORGANIZATION NAME(S) AND ADDRESS(ES) **University of Grenoble LEGI BP 53 38041 Grenoble Cedex 9 FRANCE**	8. PERFORMING ORGANIZATION REPORT NUMBER
9. SPONSORING/MONITORING AGENCY NAME(S) AND ADDRESS(ES)	10. SPONSOR/MONITOR'S ACRONYM(S)
	11. SPONSOR/MONITOR'S REPORT NUMBER(S)

12. DISTRIBUTION/AVAILABILITY STATEMENT
Approved for public release, distribution unlimited

13. SUPPLEMENTARY NOTES
See also ADM002051., The original document contains color images.

14. ABSTRACT

15. SUBJECT TERMS

16. SECURITY CLASSIFICATION OF:			17. LIMITATION OF ABSTRACT	18. NUMBER OF PAGES	19a. NAME OF RESPONSIBLE PERSON
a. REPORT	b. ABSTRACT	c. THIS PAGE			
unclassified	**unclassified**	**unclassified**	**UU**	**36**	

Subscripts

0	initial	*min*	minimum
d	desinence	*ref*	reference
i	inception	*v*	vapor
ℓ	liquid	∞	infinity

1.0 INTRODUCTION

1.1 Vapour Pressure

The development of cavitation in a liquid flow is characterized by a phase change from liquid to vapour at almost constant temperature. In the pressure / temperature chart of the fluid schematically shown in Figure 1, the red curve is the vapour pressure curve of the fluid which separates the liquid phase (in the upper left part of the diagram i.e. at low temperature and high pressure) from the vapour one (in the lower right part at high temperature and low pressure).

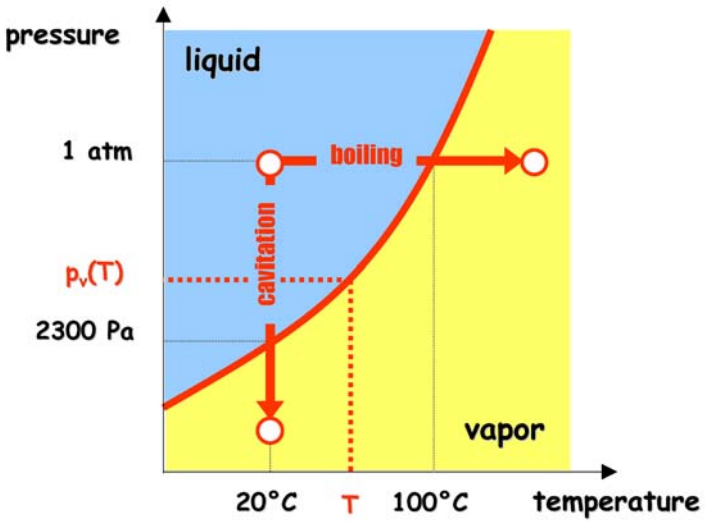

Figure 1: Schematic Phase Diagram of Water.

Cavitation is typically represented by a vertical path at constant temperature in this diagram contrary to classical boiling which corresponds to a horizontal path at constant pressure. This is a major difference between cavitation and boiling. For boiling, the driving phenomenon for phase change is an increase in temperature whereas phase change is caused by pressure reduction in the case of cavitation.

Nevertheless, there are similarities between cavitation and boiling. Figure 2 presents a typical visualization of travelling bubble cavitation on a foil section in a hydrodynamic tunnel. Cavitation appears here in the form of separate bubbles which grow on the suction side of the foil and which are similar to some extend to bubbles produced by a boiling liquid on a heated wall.

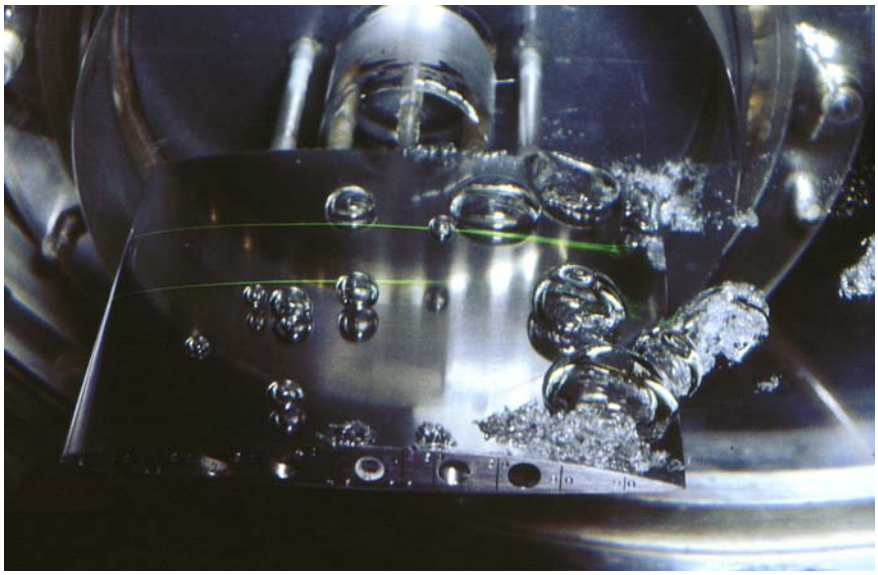

Figure 2: Travelling Bubble Cavitation on the Suction Side of a Hydrofoil in a Hydrodynamic Tunnel.

It follows that the critical parameter for the onset of cavitation is the usual vapour pressure p_v. There might be deviations and it may happen that cavitation does not appear as soon as the liquid pressure drops below the vapour pressure. As an example, surface tension brings a delay in the inception of cavitation from microbubbles carried by the liquid (cf. section 2.2). However, in most cases and particularly in industrial situations, it is a good approximation to assume that the critical pressure for the onset of cavitation is the usual vapour pressure.

1.2 Incipient and Developed Cavitation

The problem is now to understand why the pressure in a flow can drop below the vapour pressure and subsequently give rise to cavitation. As an example, consider the case of a Venturi as shown in Figure 3. This kind of Venturi with a central body is often used for the measurement of water quality (cf. section 2.3.2). Let us start the flow at a sufficiently low flowrate, so that it is everywhere free of cavitation. Velocity is obviously maximum in the section of minimum area and pressure is then minimum there, as shown by the classical Bernoulli equation:

$$p + \frac{1}{2}\rho V^2 = Constant \tag{1}$$

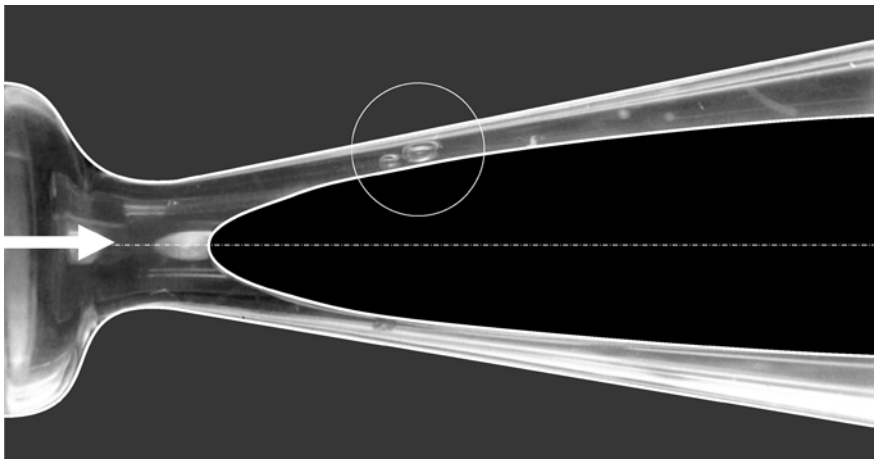

Figure 3: Cavitation Inception in a Venturi with a Central Body used for the Measurement of Nucleus Content.

Let us progressively increase the flow rate. As a consequence, the minimum pressure decreases and there will be a critical flowrate for which the vapour pressure is obtained at the throat. At this operating point, cavitation appears in the section of minimum area. In Figure 3, two bubbles are clearly visible in the upper part of the Venturi. This cavitation state is close to inception.

If the flowrate through the Venturi is further increased, the extent of cavitation increases. Figure 4 gives an example of developed cavitation in the same Venturi device. Many vapour structures which are different from single bubbles are visible.

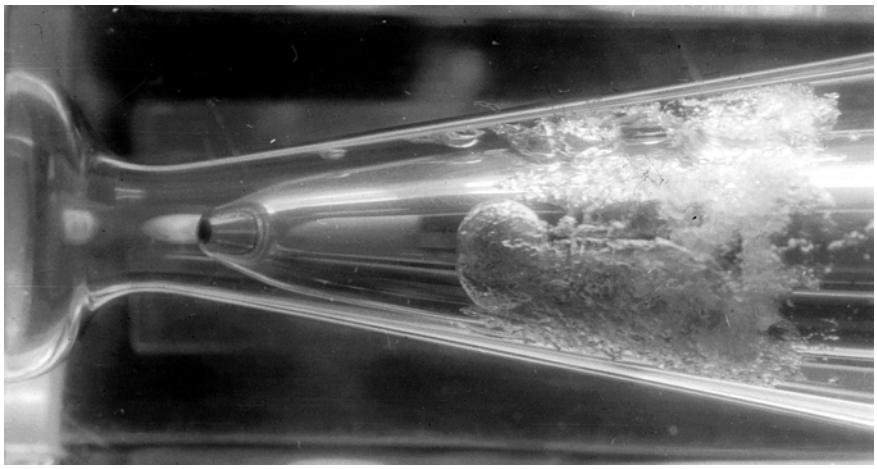

Figure 4: Developed Cavitation in the same Venturi Device as in Figure 3.

In the case of incipient cavitation (cf. Figure 3), it can reasonably be assumed that the very limited degree of development of cavitation does not affect significantly the basic fully wetted flow. Cavitation inception can then fairly well be predicted from a fully wetted flow approach.

This is no longer true for developed cavitation as it can easily be imagined because of the large volume of vapour which drastically changes the flow. It is necessary to take into account this vapour phase to correctly describe the cavitating flow. As an example, the pressure in the cavitating flow at the Venturi throat shown in Figure 4 does not decrease indefinitely as it could be expected on the basis of fully-wetted

flow considerations but remains close to the vapour pressure although the flowrate continues to be increased.

1.3 Main Cavitation Patterns

The development of cavitation in a liquid flow is characterized by the growth of vapour structures. Liquid vapour interfaces can have various shapes and the types of cavitation are often classified according to the shape of the interfaces. The following cavitation patterns are classically distinguished: travelling bubble cavitation, attached cavities, vortex cavitation and shear cavitation. They are briefly presented below.

1.3.1 Travelling Bubble Cavitation

We already mentioned the case of travelling bubble cavitation illustrated by Figure 2. This kind of cavitating flow clearly reveals weak points in the liquid from which cavitation bubbles develop. These weak points are commonly called cavitation nuclei. Microbubbles carried by the flow are typical cavitation nuclei. They are almost invisible in the liquid bulk but become macroscopic cavitation bubbles as they go through regions where the pressure drops below the vapour pressure.

The shape of such bubbles is often more complicated than purely spherical. The presence of a wall or interactions between neighbouring bubbles are reasons for deviation from the spherical shape. On Figure 2, the larger bubbles which are collapsing near the foil trailing edge are flat enough close to the wall while a hollow develops on their opposite face. This is the signature of the birth of the so-called re-entrant liquid jet which will make a hole throughout the vapour bubble and finally hit the wall.

The configuration illustrated in Figure 2 is commonly called travelling bubble cavitation since the bubbles are conveyed by the flow over the wall. They grow in the low pressure region before experiencing a collapse phase in the region of pressure recovery downstream.

1.3.2 Attached Cavitation

Another typical cavitation pattern is the attached cavity as shown in Figure 5. Contrary to travelling bubbles, such a cavity is attached to the wall in a quasi permanent way. This does not mean that the flow is steady. Actually, cavitation is almost always the source of unsteadiness which may be quite strong.

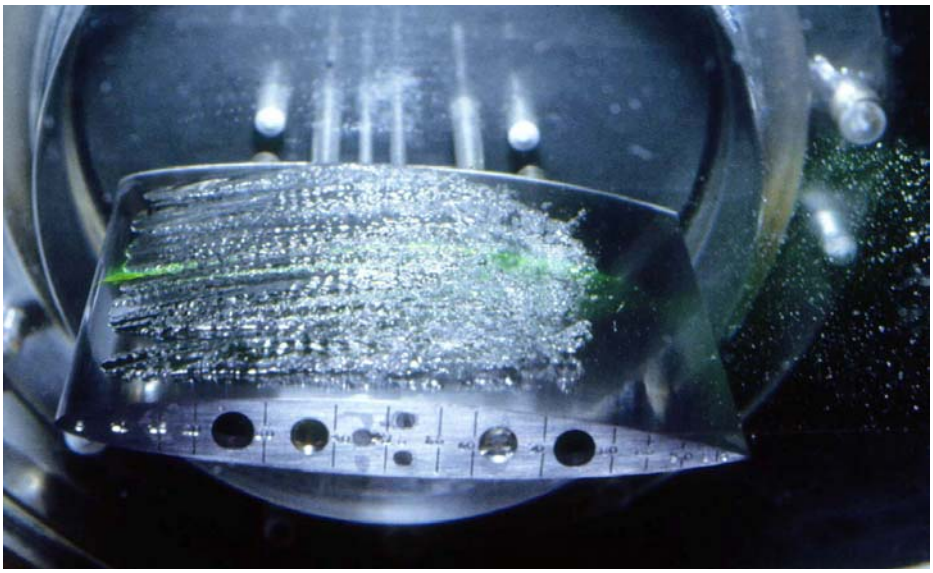

Figure 5: Leading Edge Cavity on the Suction Side of a Foil in a Hydrodynamic Tunnel.

In the present case of attached cavitation, the main source of unsteadiness originates in the rear part of the cavity. At closure, vapour structures are shed more or less periodically by the cavity and entrained by the flow. For instance, a collapsing cloud of small bubbles shed by the cavity is visible downstream the trailing edge of the foil on Figure 5. Unsteadiness is generally associated to fluctuations in cavity length which may be of large amplitude, as large as the cavity length itself in the particular case of cloud cavitation (see section 6.1).

The detachment of the cavity is generally much more stable than its closure. It is often fixed by the separation of the boundary layer (see section 5.1). As for the cavity interface, it may be glossy or frothy. In the case of Figure 5, it is smooth at detachment, which depicts a locally laminar flow, and becomes more and more rough downstream.

1.3.3 Vortex Cavitation

Figure 6 is an illustration of vortex cavitation. It is well-known that in the configuration of a 3D hydrofoil as shown in Figure 6, the pressure difference between the pressure side and the suction side of the hydrofoil generates a secondary flow which goes round the tip and gives birth to a vortex attached to the tip.

Figure 6: Vortex Cavitation Generated by a Three-Dimensional Hydrofoil.

Due to centrifugal forces, the pressure in the vortex core is lower than the pressure far away so that a minimum pressure is expected at the vortex centre. Cavitation will then develop preferably in the vortex core as shown in Figure 6. This type of cavitation is observed on marine propellers for instance which produce such a vortex at the tip of each of the blades as shown in Figure 7. Tip vortex cavitation is often the first type of cavitation observed on propellers.

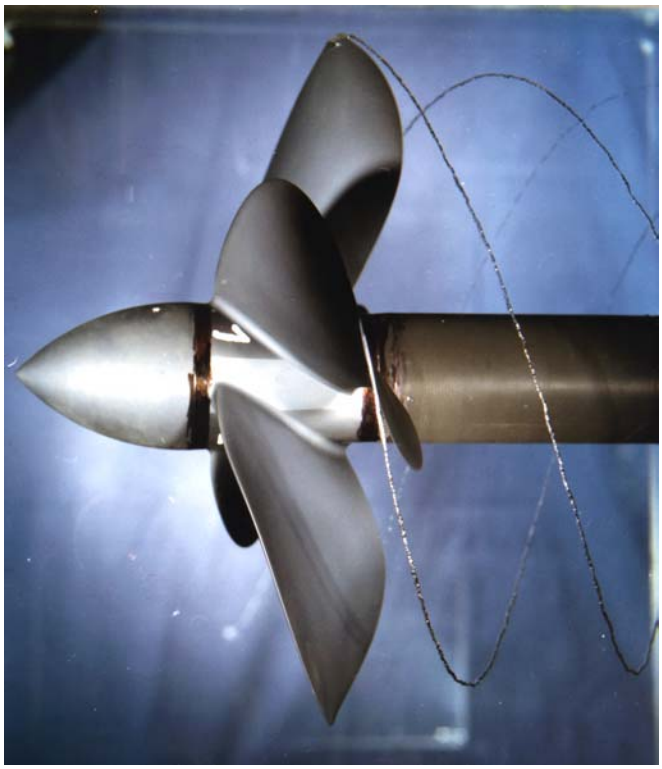

Figure 7: Vortex Cavitation Generated by a Propeller (Courtesy of DGA/BEC).

1.3.4 Shear Cavitation

The last type of cavitation considered here is shear cavitation. Such a cavitation is observed in the wake of bluff bodies or in submerged liquid jets.

Figure 8 presents a typical image of cavitation in the wake of a wedge. The turbulent wake is characterized by the existence of various types of more or less coherent vortical structures. They originate in the two shear layers which separate the wake from the main flow.

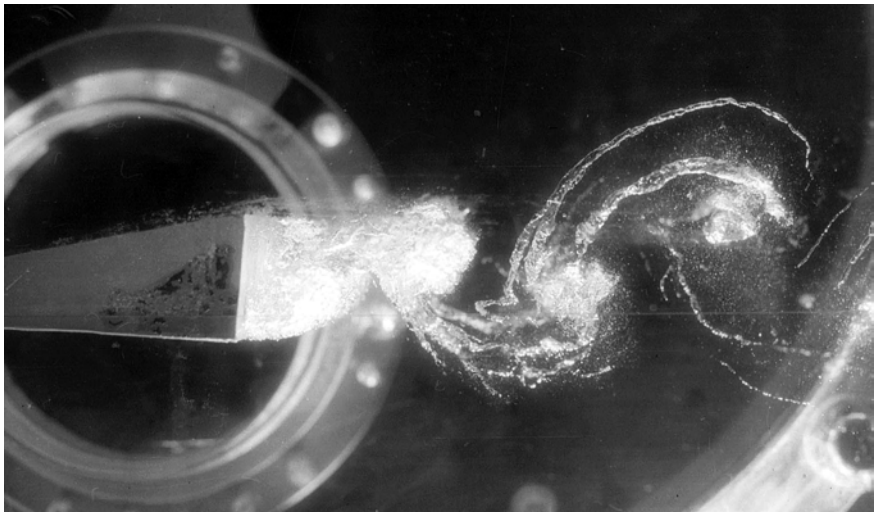

Figure 8: An Example of Cavitation in the Wake of a Bluff Body.

Similarly to the case of a well-defined tip vortex, the core of such structures is a region of low pressure where cavitation will appear first. The physics of shear cavitation is then not significantly different from that of vortex cavitation described before. The difference is essentially in the origin of the vortices and, as a consequence, in their coherence and lifetime.

In the case of submerged jets, cavitation develops in the shear layers which limit the jet and there is no fundamental difference in comparison to wakes.

Cavitation appears then as a convenient way to visualize vortices in flows and especially in turbulent flows. However, it is not a passive technique of visualization since the change from liquid to vapour induces a large change in inertia due to the large difference between liquid and vapour densities. The original fully-wetted flow will then be increasingly modified by cavitation as it develops.

As an example, in the case of turbulent wakes, the Strouhal number associated to the shedding frequency of the Von Karman vortices changes very significantly with the development of cavitation. The geometry of the wake also changes and in particular the distance between the two vortex rows is greatly modified by cavitation.

1.4 Cavitation Number

The occurrence of cavitation is determined by the condition that the minimum pressure in the flow p_{min} is lower or at least equal to the vapour pressure p_v:

$$p_{min} \leq p_v \tag{2}$$

Equality corresponds to incipient conditions.

This equation is made non-dimensional using the usual non-dimensional pressure coefficient C_p defined by:

$$C_p = \frac{p - p_{ref}}{\frac{1}{2}\rho V_{ref}^2} \tag{3}$$

where p_{ref} and V_{ref} are reference values for pressure and velocity in the flow. The choice for these values depends upon the configuration. In the case of the flow around a hydrofoil in a cavitation tunnel for instance, the reference pressure and velocity are usually chosen as the pressure and velocity far from the foil.

Using pressure coefficient, condition (2) takes the following non-dimensional form:

$$\sigma_v \leq -C_{p\,min} \tag{4}$$

where σ_v is the non-dimensional cavitation parameter defined by:

$$\boxed{\sigma_v = \frac{p_{ref} - p_v}{\frac{1}{2}\rho V_{ref}^2}} \tag{5}$$

For high values of the reference pressure (or small values of the reference velocity as well), the cavitation parameter is large and the flow is free of cavitation. Cavitation inception is obtained for the critical value:

$$\sigma_{vi} = -C_{p\,min} \tag{6}$$

Developed cavitation corresponds to values of σ_v smaller than this critical value. Therefore, the cavitation parameter can be considered as an index which measures the degree of development of cavitation.

Another critical cavitation parameter, the desinent cavitation number σ_{vd}, is also used. Parameter σ_{vd} is the critical value of σ_v at which cavitation disappears, starting from developed cavitation and progressively increasing the cavitation parameter. Because of a hysteresis effect, cavitation generally vanishes at a critical value σ_{vd} larger than σ_{vi}.

From an experimental viewpoint, the point of cavitation desinence is often considered as more repeatable than inception. In the case of tip vortex cavitation for instance, the inception of cavitation requires that a cavitation nucleus is trapped by the vortex to trigger cavitation so that the circumstances of inception of cavitation may depend upon the nuclei density. Conversely, cavitation desinence is easier to determine experimentally and measurements are generally less scattered so that the desinent cavitation number is sometimes preferred.

The σ number is a relevant scaling parameter in cavitation. For a given configuration, conservation of the cavitation number between two different operating conditions guarantees similar developments of cavitation.

Consider for example the case of a cavity attached to the leading edge of a hydrofoil at a reference pressure p_1 and a reference velocity V_1; the cavitation number is σ_1. If the velocity is changed to V_2 and the pressure adjusted to a new value p_2 so that the cavitation number is kept constant $\sigma_1 = \sigma_2$, the cavity will then have the same length. The conservation of the cavitation number ensures the similarity of both cavitating flows.

There may still remain some second-order differences between the two cavitating flows since all non-dimensional numbers are not kept constant. The Reynolds number for instance is changed and this may have an influence on cavitation. However, the conservation of the cavitation number is the first-order scaling law to be fulfilled for similar developments of cavitation.

2.0 CAVITATION NUCLEI

In Section 1.3.1, the existence of points of weakness in a liquid which behave as nuclei for the growth of the vapour phase was mentioned. The most common model of nucleus is that of a microbubble. It is presented in this section.

2.1 Equilibrium Condition

It is well-known that a liquid contains dissolved gas unless it is specially treated and deaerated. Tap water for instance contains nitrogen and oxygen from the air in proportions which are different from that existing in air.

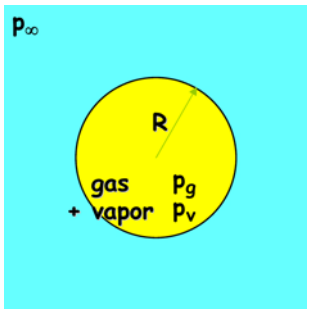

Figure 9: Microbubble in a Liquid.

When a liquid is submitted to a low pressure (as for instance if it is degassed by vacuum), microbubbles are formed. They contain non condensable gas (oxygen and nitrogen for instance) and also vapour. The partial pressure of non condensable gas inside the bubble is denoted p_g and the partial pressure of vapour is assumed to be equal to the vapour pressure. This means that thermodynamic equilibrium is assumed at the microbubble interface.

The equilibrium of pressure on both sides of the interface requires that the following condition is satisfied:

$$p_g + p_v = p_\infty + \frac{2S}{R} \tag{7}$$

This equation means that the total pressure inside the bubble $p_g + p_v$ is larger than the pressure of the liquid outside p_∞ because of surface tension S.

2.2 Critical Pressure

The problem addressed here is the determination of the equilibrium radius R as a function of the liquid pressure p_∞.

A given nucleus is characterized by a given mass of non condensable gas which is assumed constant whatever may be the evolution of the nucleus. Transfer of mass by diffusion through the interface is then ignored.

The evolution of the nucleus is supposed to be isothermal so that, using the perfect gas law, the gas pressure is inversely proportional to the bubble volume:

$$p_g = \frac{K}{R^3} \tag{8}$$

Constant K is a characteristic of the considered nucleus. It is proportional to the mass of non condensable gas enclosed. The isothermal transformation requires that the evolution of the nucleus be much slower than heat transfer, so that the temperature equilibrium is continuously achieved.

Using previous equation (8), equilibrium condition (7) is re-written as follows:

$$\frac{K}{R^3} + p_v = p_\infty + \frac{2S}{R} \tag{9}$$

For any nucleus characterized by a given value of K, Equation (9) allows the computation of the equilibrium radius R for any pressure p_∞. The corresponding equilibrium curve is shown in Figure 10.

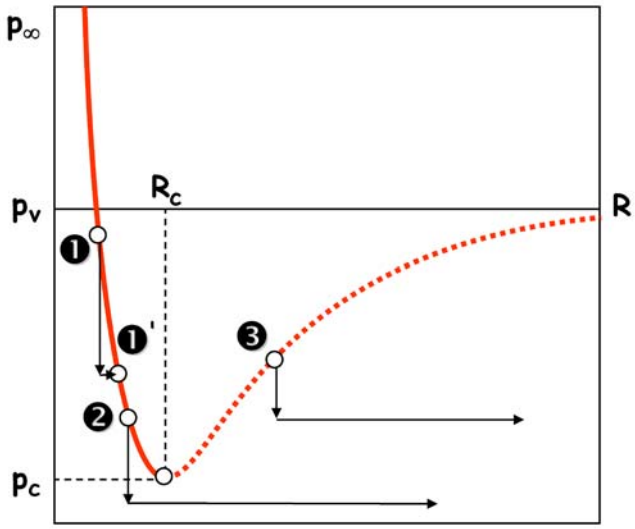

Figure 10: Radius of Equilibrium of a Microbubble as a Function of Pressure.

A remarkable feature of the equilibrium curve is the existence of a minimum defined by the following values of radius and pressure:

$$\begin{cases} R_c = \sqrt{\dfrac{3K}{2S}} \\ p_c = p_v - \dfrac{4S}{3R_c} \end{cases} \tag{10}$$

These values are called critical for reasons which will become clear from the considerations below.

The left part of the curve (solid line) corresponds to stable equilibrium. Consider the nucleus whose representative point is ❶ on the equilibrium curve and suppose that the liquid pressure is, for instance, slightly decreased. It is reasonably expected that the microbubble will grow. Its radius will increase and a new equilibrium condition will be reached at point ❶'.

Conversely, nucleus ❸ will indefinitely grow after even a slight decrease in pressure since the equilibrium curve will never be crossed again. The dotted part of the equilibrium curve is then clearly unstable.

Furthermore, if a nucleus represented by point ❷ undergoes a pressure drop below the minimum p_c defined by equation (10), the nucleus also grows indefinitely without reaching a new equilibrium and forms a cavitation bubble. The p_c value can then be interpreted as a critical value for the nucleus. If the applied pressure p_∞ is lower than this critical pressure p_c, the nucleus is destabilized and becomes a macroscopic bubble.

This model clearly shows that the critical pressure for the onset of cavitation from microbubbles is not exactly the vapour pressure. It is somewhat smaller as shown by equation (10) and the smaller the radius, the larger the deviation. This delay in the inception of cavitation is due to surface tension.

In a liquid sample where a large variety of nuclei exist, it is of common use to define the susceptibility pressure as the critical pressure of the largest nuclei (see also section 5.3). The susceptibility pressure of tap water is close to the vapour pressure because of the presence of large enough nuclei. This is the reason why it is generally stated that the critical pressure for cavitation is the usual vapour pressure. However, the present model clearly shows that deviations can be expected according to the liquid quality in terms of nuclei content.

2.3 Nuclei Control

In the 80's, experiments conducted on similar foils but in different cavitation tunnels have shown that the results of cavitation tests, cavitation inception for instance, can be very scattered. This was explained by differences in the water quality due to differences in tunnel designs and operating procedures. Special devices have then been developed to control the water quality by seeding it with nuclei. A typical seeding and measuring device is presented in this section as an example.

It must be kept in mind that all types of cavitations are not affected equally by nuclei. If travelling bubble cavitation is obviously very sensitive to nuclei, leading edge cavities are almost insensitive to water quality as discussed in section 5.2.

2.3.1 A Typical Nuclei Injection Device

Usually, without any special control, water in a cavitation tunnel is deaerated and its quality may not be representative of the actual operating conditions of the prototype. It is the reason why cavitation tunnels are often equipped with nuclei injection devices in order to reproduce as much as possible real operating conditions.

Figure 11 gives an example of such a device. Normally, water is first strongly deaerated. A proper deaeration is usually obtained by running the facility during a certain time at high velocity and low pressure so that cavitation is largely developed in the test section and deaeration by the vacuum pump is most efficient. Water quality is then controlled by injecting an adjustable number of nuclei in this deaerated water.

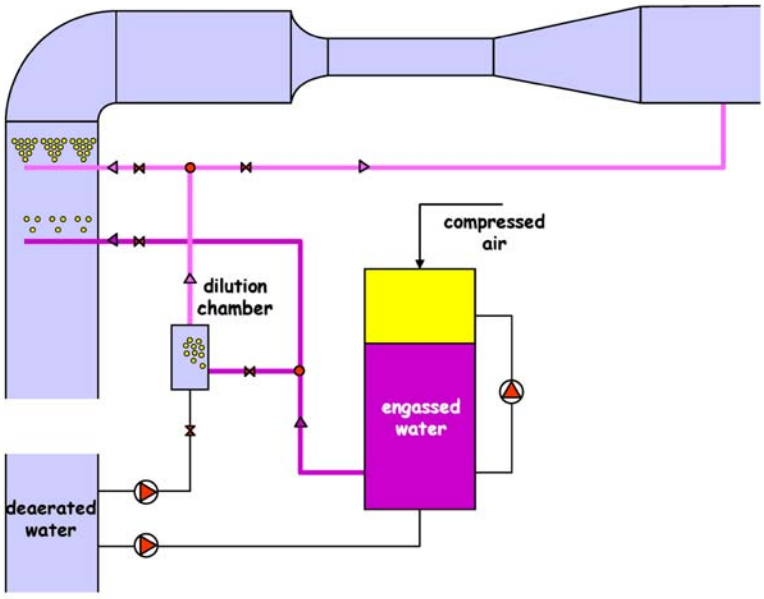

Figure 11: Typical Nuclei Injection Device.

A special tank is used to produce strongly engassed water. Basically, water in the tank is in contact with air at high pressure (a few bar for instance) so that air dissolves into water. The higher the pressure, the higher the concentration of dissolved air.

The engassed water is then injected through special cavitating injectors into the cavitation tunnel (Figure 12). Since the tunnel is running at relatively low pressure, nuclei are spontaneously produced by depressurisation of engassed water. The number of injected nuclei is controlled from the flowrate of engassed water discharged in the tunnel. Injection is generally made in the inlet duct, not too far from the test section in order to preserve the quality of nuclei and limit effects like coalescence or dissolution.

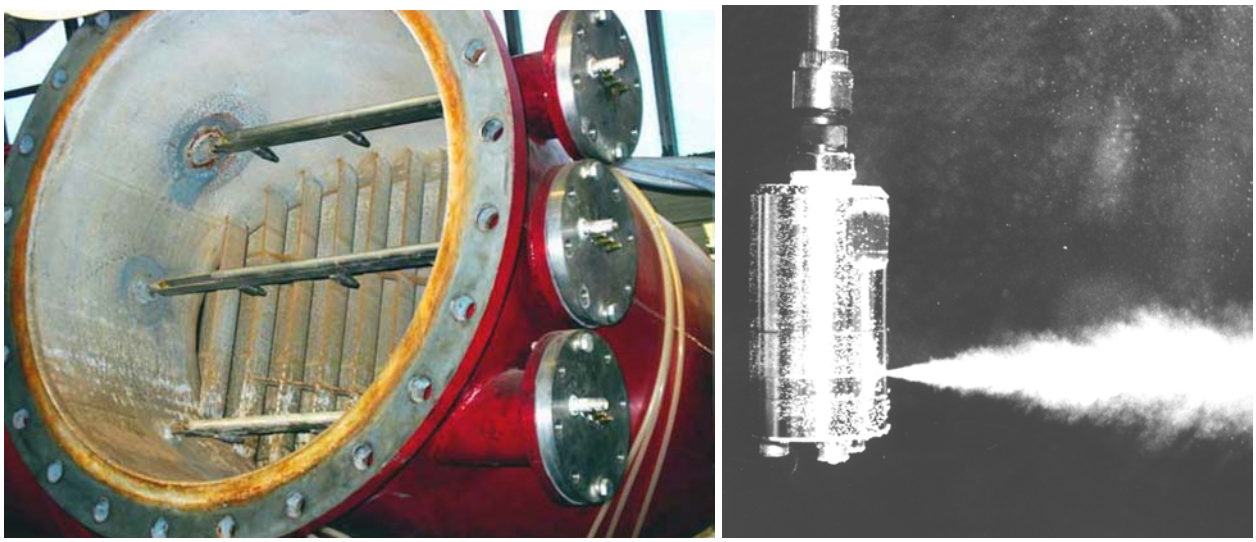

Figure 12: Injectors Mounted in the Hydrodynamic Tunnel of the University of Grenoble (left) and View of a Nuclei Injector in Operation Developed at IMHEF, Lausanne (right).

The injection device can be completed by a dilution chamber which mixes engassed water with deaerated water from the tunnel in variable proportion in order to obtain smaller nuclei concentrations. With such a device, nuclei concentration can be changed in quite a large range and this may have a strong influence on cavitation.

2.3.2 A Typical Nuclei Measuring Device

Once nuclei have been injected in the tunnel water, it is important to measure their characteristics in terms of critical pressure (or size) and concentration. Roughly speaking, we can distinguish optical methods (as holography) which measure the size of nuclei and dynamic methods (based in particular on the use of a Venturi) which measure their critical pressure.

Each technique has its own advantages and drawbacks. An interesting feature of dynamic methods is that they use the cavitation phenomenon itself for counting the nuclei. All counted nuclei will then actually be potential sites of cavitation during tests. In addition, dynamic methods supply with the nucleus critical pressure which is of direct interest in cavitation. This counting technique can then be considered as particularly appropriate for cavitation studies. It is presented below as an example.

The principle is based on the activation of nuclei by means of a Venturi type device (cf. Section 1.2). Water is continuously drawn from the tunnel and circulates through the Venturi. To be detected, a nucleus needs to be destabilized by the minimum pressure at the Venturi throat. In other words, only the nuclei whose critical pressure is larger than the minimum pressure in the Venturi will be activated and will explode.

The measuring technique can be acoustic using a ceramics which detects the noise produced by the collapse of the bubble following its explosion. In principle, it is then possible to count all the nucleus activated during their transit through the Venturi.

In practice, nuclei measurements are conducted for various flowrates through the Venturi. The higher the flowrate, the smaller the minimum pressure at throat. Hence, when the flowrate is increased, more and more nuclei of smaller critical pressure are activated. It is then possible to obtain a spectrum or a cumulative histogram of nuclei concentration as shown in Figure 14.

To increase the measuring range of the apparatus and also limit the effect of saturation for high nuclei concentrations, it may be necessary to dilute the water sample to be measured with deaerated water free of nuclei. This is made in a dilution chamber shown in Figure 13.

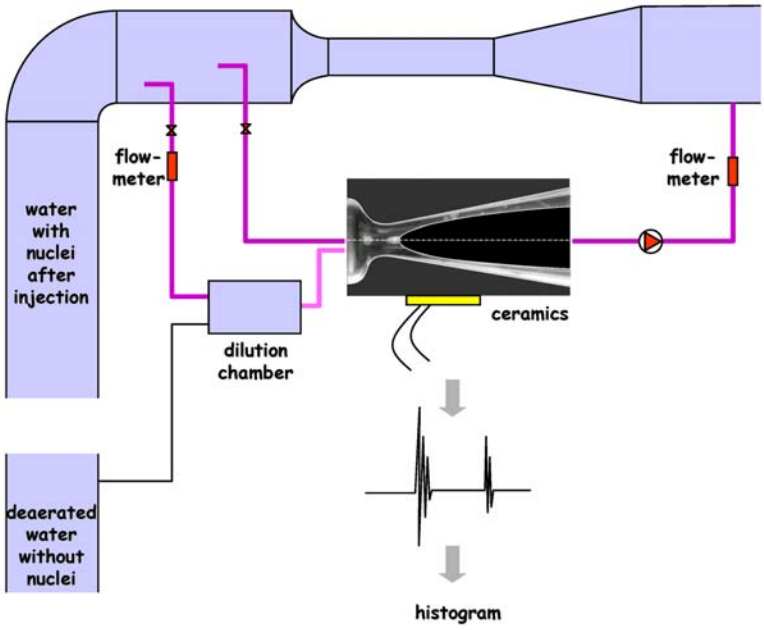

Figure 13: Typical Device using a Venturi Type Apparatus for a Dynamic Measurement of Nuclei Density.

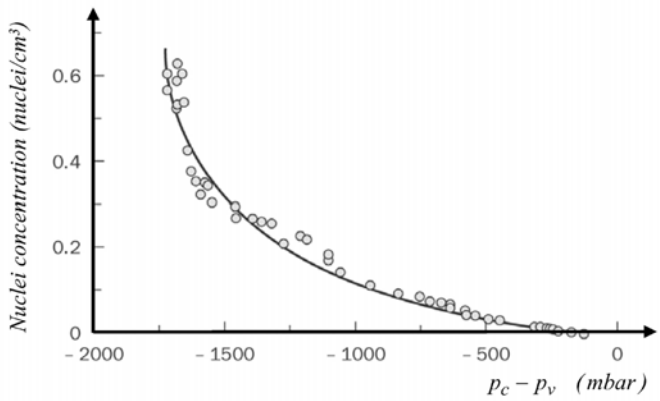

Figure 14: A Typical Nuclei Spectrum Measured with a Venturi. Each measurement point gives the number of nuclei activated by the Venturi i.e. the number of nuclei whose critical pressure is larger than the value given on the horizontal axis. The various measurements are obtained by changing the flowrate through the Venturi.

In conclusion, water quality in terms of nuclei content may strongly influence cavitation tests. Special devices have then been developed to seed water with cavitation nuclei and measure their concentration. It is sometimes chosen to systematically run cavitation tests with the highest nuclei concentration so that a kind of saturation is obtained (cf. e.g. Franc and Michel, 2004) and the test results become independent of the nuclei concentration. In addition, such a procedure generally leads to smaller performances in cavitation and guarantees a security margin for the manufacturer.

3.0 DYNAMICS OF SPHERICAL BUBBLES

In Section 2, the equilibrium of a bubble has been analysed but dynamic aspects have been ignored. Cavitating flows are however strongly affected by dynamic effects. The collapse of a cavitation bubble for instance induces very large velocities whose effects are most important.

In the basic case of a spherical bubble, the dynamics of the interface is described by the famous Rayleigh-Plesset equation. This equation is presented below together with a few typical behaviours to illustrate the importance of dynamics in cavitation.

3.1 Rayleigh-Plesset Equation

The objective is to determine the unsteady response of a bubble to liquid pressure variations. The driving term is the time evolution of the liquid pressure at infinity $p_\infty(t)$ and the output the bubble radius $R(t)$. The initial bubble radius R_0 needs to be specified as well as the initial interface velocity $\dot{R}_0$ often chosen equal to zero as it is the case if the bubble is initially in equilibrium.

The liquid is at rest at infinity and the movement induced in the liquid by the growth or collapse of the bubble is purely radial with a velocity $v(r,t)$ depending upon distance r from the bubble centre and upon time t. At the interface, we have obviously $v(R,t)=\dot{R}(t)$.

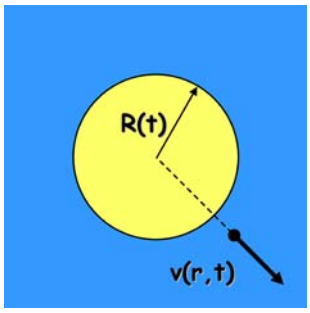

Figure 15: Bubble in a Liquid.

As in Section 2, the bubble is supposed to contain vapour at a partial pressure equal to the vapour pressure p_v and non condensable gas at partial pressure $p_g(t)$. The mass of gas is still supposed constant.

Since we are more especially concerned here by rapid evolutions (contrary to Section 2 devoted to equilibrium), we will assume that the pressure change is so rapid that heat transfer has not enough time to operate. In other words, the transformation of the gas is supposed adiabatic, and not isothermal as in Section 2. The instantaneous gas pressure $p_g(t)$ is then related to the initial gas pressure p_{g0} by the following relation:

$$p_g(t) = p_{g0}\left[\frac{R_0}{R(t)}\right]^{3\gamma} \tag{11}$$

where γ is the ratio of the heat capacities of the gas. The isothermal case is accounted for by setting parameter γ to 1.

When taking into account dynamic effects, the balance of normal forces at the bubble interface writes:

$$p_g(t) + p_v = p(R,t) + \frac{2S}{R} - 2\mu\left.\frac{\partial v}{\partial r}\right|_{r=R} \tag{12}$$

This equation is very similar to equilibrium condition (7) except that there is an extra term, the last one, which accounts for a dynamic effect since flow velocity appears. This term is the usual contribution of the viscous stress to the total normal stress at the interface.

The mass conservation equation for the liquid $div\,\vec{V} = 0$ allows the computation of the flow velocity from the interface velocity $\dot{R}$:

$$v(r,t) = \dot{R}\frac{R^2}{r^2} \tag{13}$$

It is assumed here that the liquid is incompressible. This is true as long as the flow velocity remains small in comparison with the speed of sound. In some cases and particularly at the end of the collapse phase, we will see that this condition may not be satisfied and that bubble dynamics may be affected by liquid compressibility with the emission of shock waves for example. Compressibility effects are not considered here.

Pressure gradient in the liquid can be computed from the radial projection of Navier-Stokes equation:

$$-\frac{1}{\rho}\frac{\partial p}{\partial r} = \frac{\partial v}{\partial t} + v\frac{\partial v}{\partial r} \tag{14}$$

Although the liquid viscosity is actually taken into account in the model, no viscous term appears explicitly in this equation. This is due to the type of flow which is that of a source (or sink). Using expression (13) of the flow velocity, it can easily be shown that the viscous term in the Navier-Stokes equation is always zero.

Integrating equation (14) between radius r and infinity and using expression (13) of the flow velocity, the pressure distribution in the liquid can be obtained:

$$\frac{p(r,t) - p_\infty(t)}{\rho} = \ddot{R}\frac{R^2}{r} + 2\dot{R}^2\left[\frac{R}{r} - \frac{R^4}{4r^4}\right] \tag{15}$$

On the bubble interface, pressure is then:

$$\frac{p(R,t) - p_\infty(t)}{\rho} = R\ddot{R} + \frac{3}{2}\dot{R}^2 \tag{16}$$

and the balance of normal forces on the interface (12) finally gives the famous Rayleigh-Plesset equation:

$$\rho\left[R\ddot{R}+\frac{3}{2}\dot{R}^2\right]=\left[p_v-p_\infty(t)\right]+\ p_{g0}\left[\frac{R_0}{R}\right]^{3\gamma}-\frac{2S}{R}\ -\ 4\mu\frac{\dot{R}}{R} \tag{17}$$

This differential equation allows the computation of the temporal response of the bubble radius $R(t)$ to any evolution $p_\infty(t)$ of the liquid pressure. On the right hand side, one finds the pressure term which is the driving one together with three other terms which take into account respectively the effects of non-condensable gas, surface tension and liquid viscosity. The term on the left-hand side represents the liquid inertia. If dynamic effects are ignored, i.e. if all time derivatives are set to zero, the Rayleigh-Plesset equation reduces to the classical equilibrium condition (9) (with $K=p_{g0}R_0^{\ 3}$ and $\gamma=1$ to switch from an adiabatic to an isothermal transformation).

3.2 Special Forms of the Rayleigh-Plesset Equation

Using the following identity:

$$R\ddot{R}+\frac{3}{2}\dot{R}^2=\frac{1}{2\dot{R}R^2}\frac{d(\dot{R}^2R^3)}{dt} \tag{18}$$

the Rayleigh-Plesset equation can be transformed as follows:

$$\frac{d(\dot{R}^2R^3)}{dt}\ =\frac{2}{3}\frac{p_v-p_\infty(t)}{\rho}\frac{dR^3}{dt}-\frac{2}{3(\gamma-1)}\frac{p_{g0}}{\rho}R_0^{\ 3\gamma}\frac{dR^{3(1-\gamma)}}{dt}-\frac{2S}{\rho}\frac{dR^2}{dt}\ +\ 8\nu R\dot{R}^2 \tag{19}$$

This form of the Rayleigh-Plesset equation is particularly interesting in the case where p_∞ is constant and if, in addition, viscous effects are ignored. If so, previous equation can be integrated once to give:

$$\dot{R}^2=\frac{2}{3}\frac{p_v-p_\infty}{\rho}\left[1-\frac{R_0^{\ 3}}{R^3}\right]+\frac{2}{3(\gamma-1)}\frac{p_{g0}}{\rho}\frac{R_0^{\ 3}}{R^3}\left[1-\left(\frac{R_0}{R}\right)^{3(\gamma-1)}\right]-\frac{2S}{\rho R}\left[1-\frac{R_0^{\ 2}}{R^2}\right] \tag{20}$$

Let us observe that the viscous term cannot be integrated analytically. This is the reason why it was dropped. Generally speaking, the effect of viscosity is minor in the dynamics of cavitation bubble excepts for very small bubbles so that this assumption is usually acceptable in cavitation studies.

To derive equation (20), it was assumed that the initial interface velocity $\dot{R}_0$ is zero.

3.3 Typical Behaviours

3.3.1 Collapse of a Pure Vapour Bubble

We consider here a bubble containing only pure vapour i.e. without non condensable gas inside ($p_{g0}=0$). Furthermore, we will ignore the effect of surface tension. Like for viscosity, this is usually acceptable in cavitation unless the bubble is very small, of the order of a few microns in diameter only. In equation (20), only the first term on the right hand side is then considered. This is the pressure term which is the driving term for the bubble collapse.

Equation (20) allows the computation of the bubble interface velocity:

$$\dot{R} = -\sqrt{\frac{2}{3}\frac{p_\infty - p_v}{\rho}\left[\frac{R_0^3}{R^3} - 1\right]} \tag{21}$$

Collapse clearly requires that $p_\infty > p_v$. Then $\dot{R} < 0$ and $R < R_0$ at any time. The interface velocity $\left|\dot{R}\right|$ continuously increases and tends to infinity at the end of the collapse when the bubble radius vanishes. Hence, the fluid velocity on the interface also becomes singular. This is a limitation of this simple model which obviously needs to be improved at the end of the collapse by taking into account compressibility effects.

Nevertheless, it gives a good estimate of the lifetime of a collapsing bubble. By integrating equation (21), the collapse time τ or Rayleigh time can be computed:

$$\tau = \sqrt{\frac{3}{2}\frac{\rho}{p_\infty - p_v}} \int_0^{R_0} \frac{dR}{\sqrt{\frac{R_0^3}{R^3} - 1}} \cong 0.915\, R_0 \sqrt{\frac{\rho}{p_\infty - p_v}} \tag{22}$$

As an example, a bubble of initial diameter $2R_0 = 1cm$ collapses under the atmospheric pressure $p_\infty = 10^5\, Pa$ within 460 µs. The collapse time is then small and the corresponding velocities large. When the radius is 20 times smaller than the initial radius ($R/R_0 = 1/20$), the interface velocity is about 730 m/s from equation (21), i.e. about half the speed of sound in water. The assumption of incompressibility is highly questionable and it is clear that the model needs to be improved by incorporating compressibility effects.

As for the pressure field inside the liquid during collapse, it can be computed using equation (15) and expression (21) of the interface velocity. The result of the calculation is the following:

$$\Pi(r,t) = \frac{p(r,t) - p_\infty}{p_\infty - p_v} = \frac{R}{3r}\left[\frac{R_0^3}{R^3} - 4\right] - \frac{R^4}{3r^4}\left[\frac{R_0^3}{R^3} - 1\right] \tag{23}$$

where Π is the pressure in the liquid written in a non-dimensional form. It is remarkable to observe that pressure exhibits a maximum close to the bubble wall as shown in Figure 16 which increases continuously during collapse.

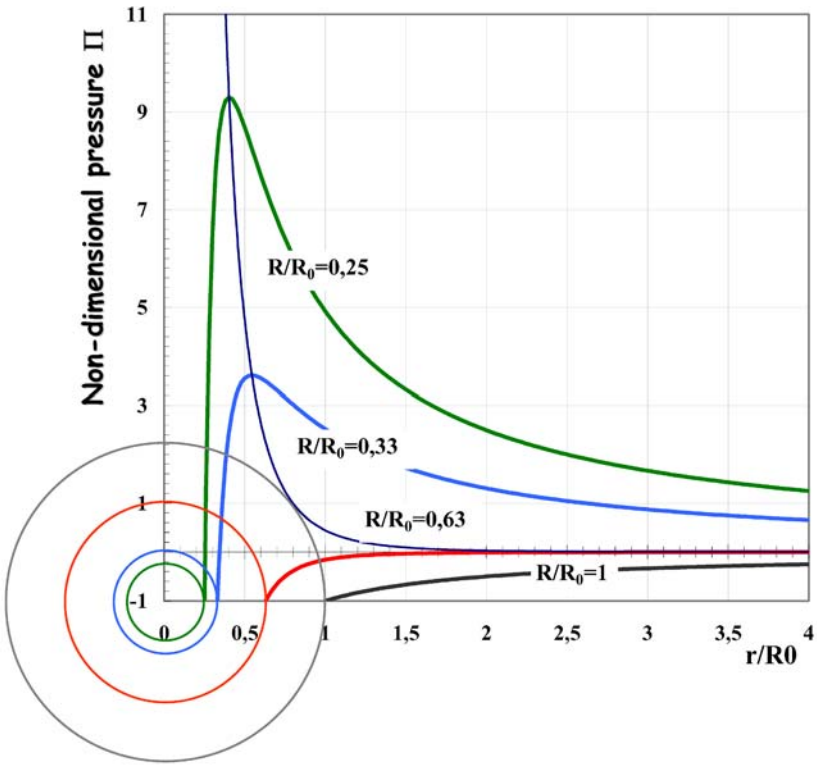

Figure 16: Non Dimensional Pressure Distribution in the Liquid during the Collapse of a Bubble.

Still for $R/R_0 = 1/20$, maximum is reached at $r/R \cong 1.59$ and is $\Pi \cong 1259$. If the bubble collapses under atmospheric pressure $p_\infty = 10^5 Pa$, the actual maximum pressure is 123 MPa at this particular instant of the collapse corresponding to $R/R_0 = 1/20$ and the maximum continues to increase with time.

Although the model needs to be improved to correctly account for the final stage of collapse, it shows, at least qualitatively, that the collapse of a bubble can generate a pressure pulse of very high amplitude comparable to yield strength and ultimate strength of usual materials, so that damage can be expected by cavitation.

The violence of collapse of a pure vapour bubble is due to the fact that pressure inside the bubble is equal to the vapour pressure which is quite small. Then, the bubble offers almost no resistance to the liquid which accelerates and converges towards the bubble centre, generating there a high concentration of energy in a small area.

The present model points out several major characteristics of the pressure loads due to cavitation bubble collapse: high amplitude, small duration and small size of the impacted area. These factors have a primary importance when considering the response of the material and subsequent possible erosion of the wall.

If the bubble holds non condensable gas, it will be compressed during collapse and will partly resist to the inward liquid motion. The collapse will be damped and the bubble may rebound after often splitting into smaller structures.

During the final stage of collapse, vapour itself may behave as non-condensable to some extend. This is due to the fact that the collapse velocity may be so large that phase change may not have enough time to operate. The importance of the phenomenon can be evaluated by comparing the relative order of

magnitude of the characteristic time of collapse to that of the kinetics of condensation (Fujikawa and Akamatsu, 1980).

3.3.2 Explosion of a Nucleus

When exposed to a pressure lower than its critical pressure, a nucleus explodes and becomes a macroscopic cavitation bubble. In this section, we will compute the growth rate of the bubble which could not be estimated from the stability analysis developed in section 2.2.

As soon as the original microbubble becomes a macroscopic bubble with a change in radius of several orders of magnitude, the effects of non condensable gas as well as that of surface tension are negligible. For large values of R ($R \to \infty$), the two corresponding terms actually vanishe in equation (20) which takes the following asymptotic form:

$$\dot{R} \cong \sqrt{\frac{2}{3}\frac{p_v - p_\infty}{\rho}} \tag{24}$$

This is the asymptotic growth rate of a cavitation bubble under pressure $p_\infty < p_v$. It is representative for instance of the growth rate of bubbles in travelling bubble cavitation on a foil (see Figure 2 for instance) provided that interactions between bubbles remain negligible.

3.3.3 Bubble Oscillations

Another typical behaviour of cavitation bubbles is oscillations. In section 2.1, we observed that the left hand side of the equilibrium curve (cf. Figure 10) is stable. If a bubble is in stable equilibrium and if equilibrium is perturbed, the bubble will oscillate. We show here that the resonance frequency can be estimated from equation (20).

For this purpose, equation (20) is re-written symbolically as $\dot{R}^2 = F(R)$ where function $F(R)$ can easily be identified from equation (20). If the bubble is initially in equilibrium, we have $\dot{R}_0 = \ddot{R}_0 = 0$ i.e. $F(R_0) = F'(R_0) = 0$. It can easily be checked that condition $F'(R_0) = 0$ reduces to equilibrium condition (7).

For R in the vicinity of R_0, $F'(R) \cong (R - R_0)F''(R_0)$ so that the dynamics of the cavitation bubble is governed by the following linearized equation:

$$\ddot{R} - \frac{F''(R_0)}{2}(R - R_0) \cong 0 \tag{25}$$

The type of solution depends upon the sign of the second derivative $F''(R_0)$. If $F''(R_0) > 0$, the equilibrium is unstable. It can easily be checked that this condition is equivalent to $R_0 > R_c$ where R_c is the bubble critical radius introduced in equation (10) (after setting γ to unity in order to switch from an adiabatic to an isothermal transformation). Hence, the equation of dynamics confirms that the right hand side of the equilibrium curve is unstable.

On the other hand, if $F''(R_0) < 0$, equation (25) shows that the bubble oscillates sinusoidally around equilibrium. Equilibrium is stable and the frequency of oscillation i.e. the bubble resonance frequency is:

$$f = \frac{1}{2\pi}\sqrt{\frac{-F''(R_0)}{2}} \tag{26}$$

By computing the second derivative of F from equation (20), we obtain the following expression of the bubble resonance frequency:

$$f = \frac{1}{2\pi R_0}\sqrt{\frac{1}{\rho}\left[3\gamma p_{g0} - \frac{2S}{R_0}\right]} = \frac{1}{2\pi R_0}\sqrt{\frac{1}{\rho}\left[3\gamma\left(p_{\infty 0} - p_v + \frac{2S}{R_0}\right) - \frac{2S}{R_0}\right]} \tag{27}$$

The oscillations remain sinusoidal only if the original change in pressure is small enough. If not, bubble may still oscillate but its radius will not remain close to equilibrium radius R_0; big changes in radius will occur. The elastic behaviour of the non condensable gas is not the same for small and large radii: the role of gas is smaller and even negligible for large values of the radius whereas it is dominating for small radii. This brings a dissymmetry in the oscillation which is no longer sinusoidal (cf. Figure 17).

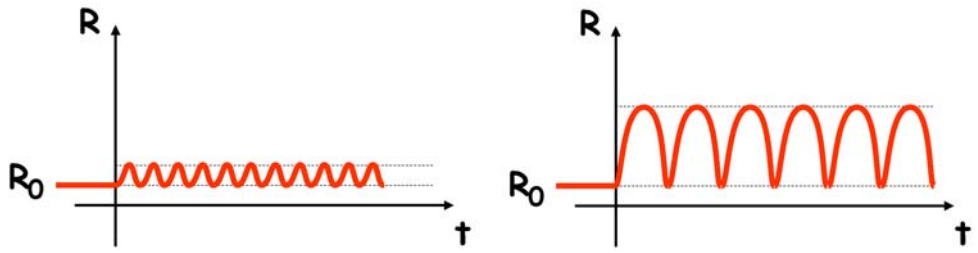

Figure 17: Two Typical Regimes of Oscillation of a Bubble Subjected to a Pressure Drop at Time t=0. When the pressure drop is relatively small, oscillations are sinusoidal (left) whereas they become asymmetric for a larger pressure drop.

Here, viscous effects were not taken into account and no dissipation occurs. In practice, viscosity has a damping effect on oscillations so that the amplitude of oscillation decreases. The effect of damping by viscosity is more important for small radii.

4.0 THERMAL EFFECTS IN CAVITATION

In the introduction of this chapter (section 1.1), it was mentioned that phase change occurs at constant temperature in cavitation. This is generally a good approximation. In the case of water at room temperature for instance, the temperature difference due to phase change is extremely small.

In other fluids, sometimes called thermosensitive, cavitation is accompanied with a non negligible temperature drop. The phenomenon depends greatly upon the physical properties of the fluid (latent heat of vaporisation, heat capacity, ratio of liquid to vapour density, heat conductivity…). This is particularly the case of cryogenic liquids used for rocket engine propulsion as liquid hydrogen for which a temperature depression of the order of a few degrees appears with the development of cavitation.

The approach presented here is a phenomenological analysis based on a bubble type model. It is basically a dimensional approach devoted to point out key parameters in the analysis of thermal effects in cavitation.

4.1 Heat Balance and B-factor

The reason for the temperature drop inside the cavities is easy to understand. The production of a volume V_v of vapour requires the quantity of heat $\rho_v V_v L$ to be supplied (L is the latent heat of vaporization).

This energy is supplied by the liquid in the vicinity of the cavitation region which will then be cooled. This is the reason why the temperature of the liquid neighbouring the cavitating zone and the two-phase region itself are at a lower temperature.

Following Stepanov (1964), we introduce the volume of liquid V_ℓ which supplies the heat for vaporization. Assuming its temperature drop is ΔT, the heat balance writes as follows:

$$\rho_v V_v L = \rho_\ell V_\ell c_{p\ell} \Delta T \tag{28}$$

where ρ_ℓ is the liquid density and $c_{p\ell}$ its heat capacity. The B-factor of Stepanov is defined by:

$$B = \frac{\Delta T}{\frac{\rho_v L}{\rho_\ell c_{p\ell}}} = \frac{V_v}{V_\ell} \tag{29}$$

This equation shows that a relevant parameter to make the temperature drop non dimensional is the following reference temperature difference:

$$\Delta T^* = \frac{\rho_v L}{\rho_\ell c_{p\ell}} \tag{30}$$

It depends only upon the fluid. From a physical viewpoint, it is the temperature drop to apply to a given volume of liquid in order to get the energy required for producing the same volume of vapour. Experiments show that ΔT^* is often a relevant order of magnitude of the actual temperature drop ΔT inside the cavities. The following table gives typical values of ΔT^* in the case of water and liquid hydrogen together with other parameters which will be discussed in section 4.3.

Table 1: Comparison of Thermal Data for Water and Liquid Hydrogen

Fluid	Water	Liquid Hydrogen
Temperature	20°C	22.2 K
$\frac{\rho_\ell}{\rho_v}$	58 000	31.4
ΔT^* (K)	0.010	1.25
Σ (m/s$^{3/2}$) Brennen's parameter	3.9	2.1×10^6
$\frac{\Delta p_v^*}{\rho_\ell \alpha_\ell}$ (s^{-1})	1.0×10^4	6.0×10^9

In the case of water, the reference temperature difference ΔT^* is about 0.01 K whereas it is about 1 K in liquid hydrogen.

4.2 Vapour Pressure Drop and Modified Rayleigh Equation

The drop in vapour pressure Δp_v associated to temperature depression ΔT is

$$\Delta p_v = \frac{dp_v}{dT}\Delta T \tag{31}$$

where dp_v / dT is the slope of the vapour pressure curve. It can be estimated using the famous thermodynamic equation of Clapeyron in which the vapour density can usually be neglected with respect to that of the liquid:

$$L = T\left[\frac{1}{\rho_v} - \frac{1}{\rho_\ell}\right]\frac{dp_v}{dT} \cong \frac{T_\infty}{\rho_v}\frac{dp_v}{dT} \tag{32}$$

so that:

$$\frac{dp_v}{dT} \cong \frac{\rho_v L}{T_\infty} \tag{33}$$

The reference pressure drop Δp_v^* corresponding to the reference temperature drop ΔT^* is defined by:

$$\Delta p_v^* = \frac{dp_v}{dT}\Delta T^* \tag{34}$$

Consider the case of a cavitation bubble which grows due to an applied pressure $p_\infty(t)$ smaller than the vapour pressure p_v. The latter should be evaluated at the actual cavity temperature $T_\infty - \Delta T$ which is smaller than the liquid temperature far from the bubble T_∞. Its dynamics is governed by the Rayleigh Plesset equation (17):

$$\rho\left[R\ddot{R} + \frac{3}{2}\dot{R}^2\right] = p_v(T_\infty - \Delta T) - p_\infty(t) \tag{35}$$

provided the actual vapour pressure $p_v(T_\infty - \Delta T)$ is used. In equation (35), only the driving term connected to the applied pressure was kept. The effects of non condensable gas, surface tension and viscosity were ignored in a first step.

Since $p_v(T_\infty - \Delta T)$ is smaller than $p_v(T_\infty)$, it follows that bubble growth is somewhat slowed down. This is a general conclusion regarding thermal effects which tend to reduce the development of cavitation.

By introducing the drop in vapour pressure (31) in previous equation, we get the following modified Rayleigh equation:

$$\boxed{\rho\left[R\ddot{R} + \frac{3}{2}\dot{R}^2\right] + \frac{dp_v}{dT}\Delta T = p_v(T_\infty) - p_\infty(t)} \tag{36}$$

The second term on the left hand side accounts for thermal effects.

4.3 Estimation of Temperature Depression

The major problem is to estimate the heat supplied by the liquid surrounding the bubble. Brennen (1994, 1995) assumes that heat transfer is achieved by pure conduction in the liquid. This assumption looks

reasonable if the bubble is travelling with the liquid without slip. However, other investigators using a different approach based on the consideration of an attached cavity noticed that heat transfer is greatly enhanced by turbulence and were obliged to artificially increase the liquid thermal diffusivity by several orders of magnitude to get reasonable predictions (Kato 1984, Watanabe et al. 2005).

The problem of heat transfer at the interface in cavitating flows is still open. Heat transfer is modelled here by a convective approach assuming that heat flux φ at the interface is proportional to the temperature difference ΔT :

$$\varphi = h\,\Delta T \tag{37}$$

The convective coefficient h is considered here as a free parameter. Usual correlations on convective heat transfer can be tried although there is no guarantee of their applicability to cavitation. Fruman et al. (1999) have shown that they can give good results provided the roughness of the interface is taken into account.

Temperature depression is estimated from a heat balance. The heat flux (37) supplied by liquid at the interface balances the heat required for vaporization and growth of the bubble, i.e.:

$$h\,\Delta T\,(4\pi R^2) = \frac{d}{dt}\left(\frac{4}{3}\pi R^3\right)\rho_v L \tag{38}$$

Temperature depression is then given by:

$$\boxed{\Delta T = \frac{\rho_v L}{h}\dot{R}} \tag{39}$$

It is proportional to the bubble growth rate. If the bubble grows, ΔT is positive whereas, if the bubble shrinks, heat is recovered by the liquid because of condensation and ΔT is negative.

4.4 Criterion for Thermal Effects

By introducing this estimate of ΔT in Rayleigh equation (36), we finally obtain the following differential equation which governs the dynamics of a bubble when thermal effects are included:

$$\boxed{\rho\left[R\ddot{R}+\frac{3}{2}\dot{R}^2\right]+\frac{dp_v}{dT}\frac{\rho_v L}{h}\dot{R} = p_v(T_\infty)-p_\infty} \tag{40}$$

The second term on the left hand side is still the thermal term.

For discussion, equation (40) is made non dimensional using a characteristic length scale D and a characteristic velocity V of the flow. Transit time $\tau = D/V$ is used as the reference time for bubble evolution. The non dimensional form of equation (40) is then:

$$\boxed{\left[\bar{R}\ddot{\bar{R}}+\frac{3}{2}\dot{\bar{R}}^2\right]+\frac{1}{Nu}\frac{\Delta p_v^*}{\rho_\ell\,\alpha_\ell}\tau\,\dot{\bar{R}} = \frac{-C_p-\sigma_v}{2}} \tag{41}$$

where upper bars hold for non-dimensional quantities. Parameter $\Delta p_v^*/\rho_\ell\,\alpha_\ell$ is the inverse of a time. It depends only upon the fluid properties. Using equations (34), (33) and (30), it can be written as follows:

$$\frac{\Delta p_v^*}{\rho_\ell \alpha_\ell} \cong \frac{(\rho_v L)^2}{\rho_\ell{}^2 c_{p_\ell} T_\infty \alpha_\ell} \tag{42}$$

This parameter is very similar to Brennen's parameter Σ (Brennen 1994, 1995) except that thermal diffusivity appears to power 1 instead of 0.5. The difference is due to the fact that present approach is based upon a convective model contrary to the conductive approach of Brennen. Anyway, this parameter appears recurrently in models of thermal effects with possible minor changes. Kato (1984) also introduced a very similar parameter although his model considers an attached cavity instead of a bubble.

The value of this parameter is given in Table 1 for water and liquid hydrogen as a reference. It is much larger in liquid hydrogen than in water which confirms the fact that thermal effects are much more important in liquid hydrogen.

The second term on the left hand side of equation (41), the thermal term, has to be compared to the right hand side term to evaluate the importance of thermal effects. The latter which is a combination of the cavitation number and pressure coefficient is typically of the order of unity. Therefore, the magnitude of thermal effects depends upon the factor:

$$\frac{1}{Nu} \frac{\Delta p_v^*}{\rho_\ell \alpha_\ell} \tau \tag{43}$$

It is the ratio of two characteristic times, the transit time τ and the following time:

$$\boxed{\tau_T = Nu \frac{\rho_\ell \alpha_\ell}{\Delta p_v^*}} \tag{44}$$

which can be considered as a characteristic thermal time since it contains the information on heat transfer at the interface.

If the thermal time is much larger than the transit time, thermal effects are negligible and equation (43) reduces to the usual Rayleigh equation. Conversely, if the thermal time is much smaller than the transit time, thermal effects are predominant. A suitable criterion for estimating the magnitude of thermal effects is then based on the comparison of these two characteristic times.

The thermal time depends on the ratio $\rho_\ell \alpha_\ell / \Delta p_v^*$ which is a function of fluid properties only (cf. e.g. table 1) and also on the Nusselt number which describes the intensity of heat transfer at the interface. The Nusselt number needs to be estimated. Usual correlations on convective heat transfer can be used (cf. e.g. Fruman et al. 1999) or more specific correlations can be deduced from experimental data on cavitation in thermosensitive fluids.

4.5 Scaling Laws with Thermodynamic Effects

Returning to version (41) of the Rayleigh Plesset equation which includes thermal effects, it is possible to derive the scaling laws to be satisfied between two different flows in order to ensure similar developments of cavitation when thermal effects exist.

Firstly, geometric similarity is obviously necessary in order to ensure similarity in pressure coefficient distribution C_p. The usual scaling law in cavitation number σ_v is also necessary so that the term on the right hand side of equation (41) remains the same. This is the usual cavitation scaling law in the absence of any thermal effect.

Because of thermal effects, an additional scaling law is necessary. Bubbles will have similar developments or in other words, the non dimensional solution to equation (41) will be the same, only if the non dimensional number τ / τ_T which is the coefficient of $\dot{\overline{R}}$ in the thermal term remains constant. Thus, perfect scaling requires the conservation of another non-dimensional parameter which specifically characterizes thermal effects.

However, a simplified scaling is often used. Consider for instance a given pump working (1) with water at room temperature i.e. without thermal effect and (2) with a thermosensitive fluid presenting a significant thermal effect. If both tests are conducted at the same cavitation number σ_v based on the vapour pressure at the liquid temperature at infinity $p_v(T_\infty)$:

$$\sigma_v = \frac{p_{ref} - p_v(T_\infty)}{\frac{1}{2}\rho V_{ref}^{\ 2}} \tag{45}$$

cavitation will be less developed in the thermosensitive fluid than in water because of thermal effects as shown in Figure 18.

Without thermal effect (water at room temperature, $\Delta T^* = 0.01\,K$)

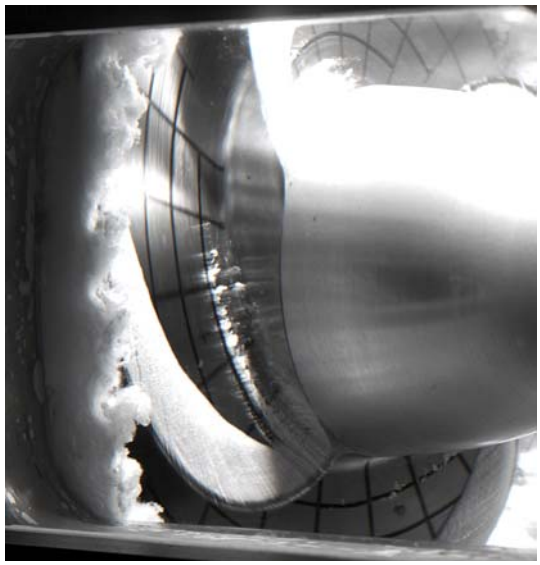

With thermal effects (Refrigerant 114 at 40°C, $\Delta T^* = 2.0\,K$)

Figure 18: Visualisation of Leading Edge Cavitation in an Inducer of Rocket Engine for the Same Cavitation Number $\sigma_v = 0.011$ but with Two Different Fluids (nominal flowrate, 5 000 rpm) (courtesy of CNES/SNECMA).

On the other hand, it is generally considered that a scaling law based on the conservation of the cavitation number σ_c calculated with the actual pressure inside the cavitating zone $p_v(T_\infty - \Delta T)$ (which is a priori unknown):

$$\sigma_c = \frac{p_{ref} - p_v(T_\infty - \Delta T)}{\frac{1}{2}\rho V_{ref}^{\ 2}} \tag{46}$$

ensures similar developments of cavitation. This is a good approximation for moderate thermal effects although perfect similarity is not ensured. In the case of a leading edge cavity for instance, differences in the relative thickness of the cavity can be expected. Anyway, the σ_c scaling law is, to the first order, a suitable scaling law when thermal effects are not negligible. Such an approach assumes that a mean temperature difference can be attached to the cavity although changes may be observed all along the cavitating zone as revealed by the present bubble-type model.

5.0 THE EFFECTS OF THE BOUNDARY LAYER AND NUCLEI CONTENT ON CAVITATION PATTERNS

Two main factors influence the type of cavitation on a wall: the water quality in terms of nuclei content and the characteristics of the boundary layer flow. A major feature of the boundary layer with respect to cavitation is separation. Roughly speaking, an attached cavity is correlated to a separated boundary layer. As for travelling bubble cavitation, it is generally associated to a non separated boundary layer and to the presence of nuclei in the liquid.

An amazing example of the influence of nuclei is given in Figure 19. The two different patterns, an attached cavity and travelling bubbles, are simultaneously present on the same hydrofoil whereas flow conditions and boundary layer flows are obviously the same. This is due to a much higher concentration in nuclei in the rear part of the test section where nuclei seeding is turned on in comparison to the front part where it is off.

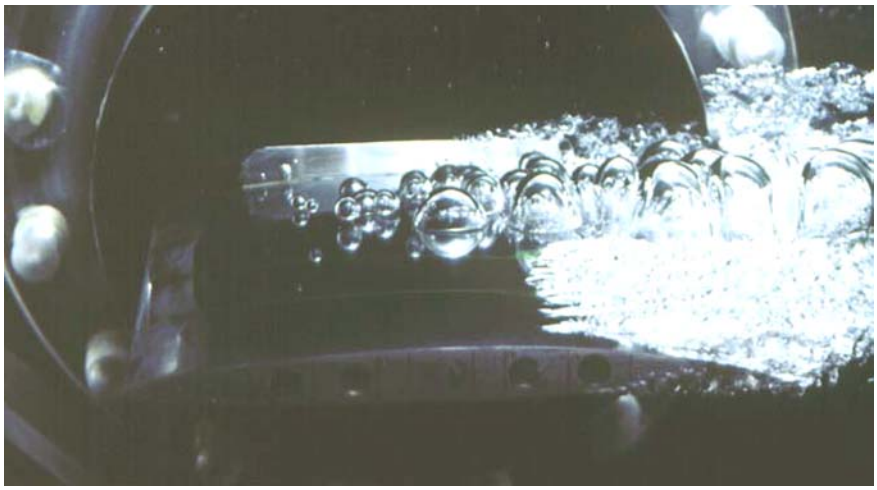

Figure 19: Illustration of the Effect of Nuclei on a Two-Dimensional Hydrofoil in a Cavitation Tunnel. Water is basically strongly deaerated and nuclei seeding is turned on only in the second half of the test section. This results in the juxtaposition of two very different kinds of cavitation although fluid flow conditions are exactly the same along the whole hydrofoil span.

Present section is devoted to a detailed analysis of the effects of boundary layer and nuclei content on cavitation patterns. Three basic configurations of the boundary layer are considered : a separated laminar boundary layer, a laminar separation bubble and an attached turbulent boundary layer. For each case, the influence of nuclei is analysed and the interaction between travelling bubble cavitation and attached cavitation are discussed. The conclusions are useful to analyse any cavitating flow but also to control cavitation patterns from the control of the boundary layer flow and the liquid quality.

5.1 Case 1: Separated Laminar Boundary Layer

The first case considered here is that of a laminar boundary layer which separates from the wall. A typical example is shown in Figure 20 for a foil at zero angle of attack. The boundary layer is visualized by dye injection at the leading edge. The separation point is clearly visible in the rear part of the foil. It is due to an adverse pressure gradient which forces separation.

Downstream separation, instabilities develop in the shear layer which limits the wake. Such instabilities are clearly visible on Figure 20. The green streak line starts to gently oscillate downstream separation and then rolls up to give birth to discrete vortical structures typical of the Kelvin-Helmholtz instability. This is the preliminary step in the transition to turbulence.

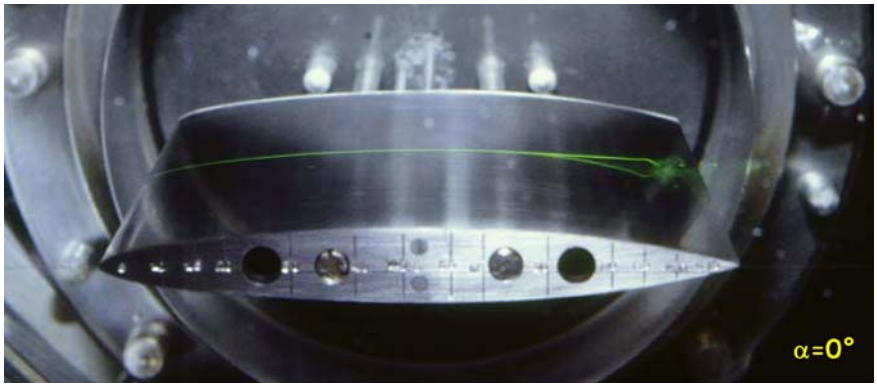

Figure 20: A Separated Laminar Boundary Layer on a Hydrofoil (fully wetted flow).

At inception, cavitation develops firstly in the core of these spanwise vortices as very schematically shown in Figure 21. This is a cavitation pattern typical of shear cavitation with a possible development of cavitation also in three-dimensional streamwise vortices, if any. The incipient cavitation number is close to the opposite of the pressure coefficient at laminar separation.

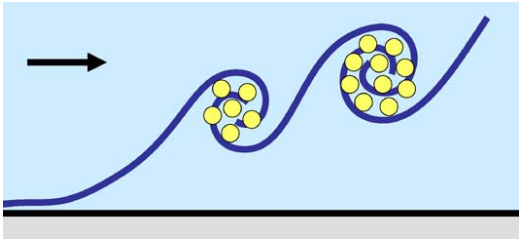

Figure 21: Cavitation Inception in the Core of Vortices due to Kelvin-Helmholtz Instability in the Shear Layer Downstream Separation (magnification of the vicinity of separation).

When cavitation number is decreased, shear cavitation transforms into an attached cavity which progressively fills up the whole separated zone as shown in Figure 22. The cavity interface is glossy close to cavity detachment which depicts a laminar flow and then becomes frothy which is the signature of transition to turbulence.

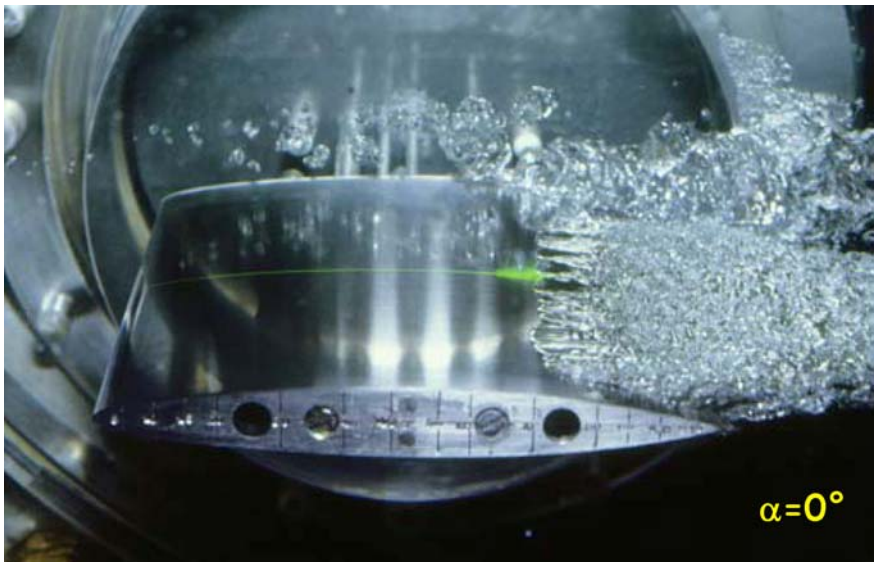

Figure 22: Attached Cavitation in the Rear Part of a Hydrofoil at Low Angle of Attack.

The comparison of Figure 20 and Figure 22 demonstrates the strong correlation between attached cavitation and laminar separation. This is a general result observed in other configurations and in particular in the case of a laminar separation bubble examined in section 5.2.

The existence of separation is the only opportunity for a cavity to be sheltered from the oncoming flow. A laminar separation region and the associated wake is a dead zone in which a cavity can develop and be in mechanical equilibrium or "attached" to the wall. If the flow is not separated, the cavity is subject to a force by the oncoming flow which will sweep it away.

The disappearance of separation is generally a consequence of transition to turbulence. It is well known that a turbulent boundary layer can withstand a larger adverse pressure gradient than a laminar one without separating. This is why transition to turbulence generally forces a separated laminar boundary layer to reattach to the wall. As a consequence, transition to turbulence has a negative effect on attached cavitation since it removes the dead zone in which the cavity could settle down and so prevents any cavity to attach to the wall.

This configuration of a trailing edge attached cavity occurs for a sufficiently low nuclei content. Pressure inside the cavity is equal to the vapour pressure. Because of separation of the boundary layer, an adverse pressure gradient exists upstream separation. Hence, there is a region of the wall, upstream cavity detachment, where pressure is necessarily smaller than the vapour pressure. If water contains nuclei, they may be activated by this low pressure zone and thus give rise to travelling bubble cavitation.

The explosion of a nucleus disturbs the boundary layer flow and often triggers a local transition to turbulence in the form of a turbulent spot. As explained above, transition to turbulence causes the reattachment of the boundary layer flow to the wall and the subsequent disappearance of the attached cavity, at least locally and temporally. This phenomenon is illustrated in Figure 23 where a hole in the trailing edge cavity is visible in the middle of the foil due to the passage of a cavitation bubble also visible downstream. A travelling cavitation bubble has then a negative effect on an attached cavity by triggering transition to turbulence.

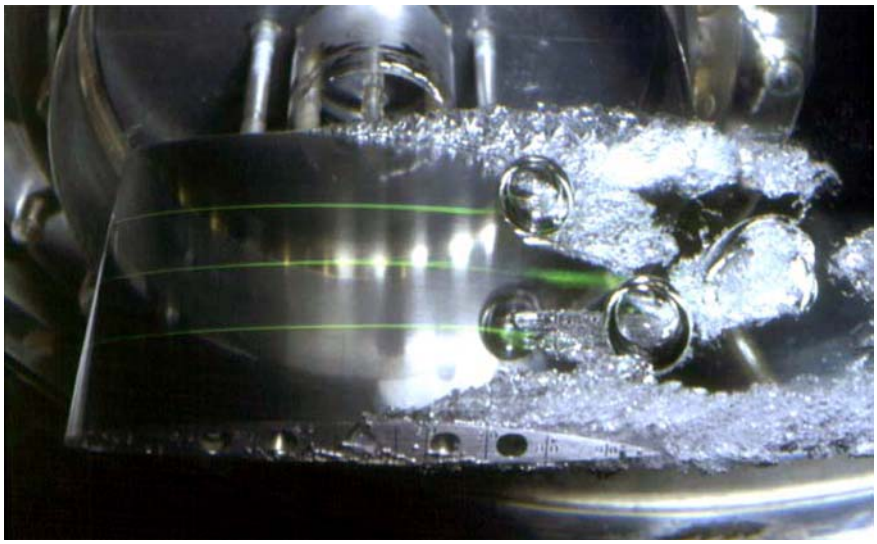

Figure 23: Effect of Travelling Bubble Cavitation on an Attached Cavity.

If the nuclei density is relatively small, cavitation bubbles explode from time to time on the wall and an intermittency is observed, in space as in time, between travelling bubble cavitation and attached cavitation. The number of travelling cavitation bubbles increases with increasing nuclei density. For a relatively large nuclei density, the trailing edge cavity will definitely disappear and be replaced by travelling bubble cavitation. This is what happens in the back of the test section in Figure 19.

From this discussion, it appears that a critical nuclei concentration exists. It corresponds to the threshold for a permanent disappearance of attached cavitation. Its order of magnitude can be estimated theoretically from the concept of saturation (Franc and Michel, 2004).

5.2 Case 2: Laminar Separation Bubble

The second configuration discussed here is the case of a laminar separation bubble. This is a very common situation on blades at relatively large angle of attack. It is illustrated in Figure 24.

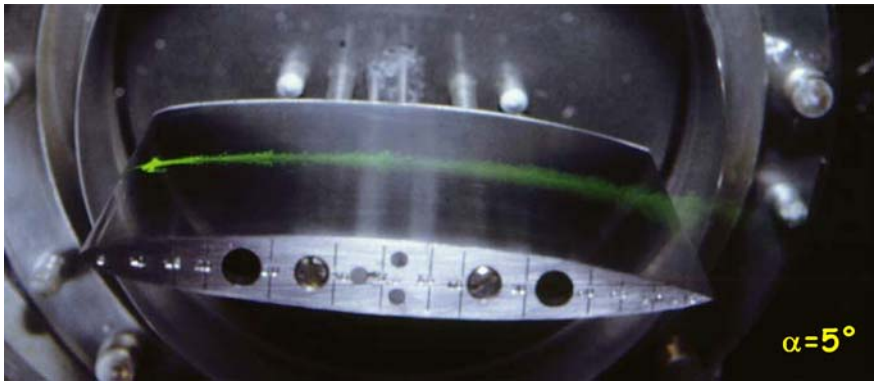

**Figure 24: Laminar Separation Bubble near the Leading Edge of a Hydrofoil.
The laminar separation bubble, which is a tiny dead water zone,
is made visible by some spreading of dye along the span.**

A laminar separation bubble is due to the adverse pressure gradient which appears near the leading edge of a foil for relatively large angles of attack. The laminar boundary layer separates in the vicinity of the

leading edge and transition to turbulence occurs very close to separation so that the turbulent boundary layer reattaches to the wall. Separation, transition and reattachment all take place in a tiny region which is precisely the laminar separation bubble. Downstream, boundary layer is turbulent and attached to the wall before separating close to the trailing edge.

Cavitation inception is characterized by the growth of nuclei trapped in this small recirculation region made of the laminar separation bubble as schematically shown in Figure 25. They give birth to a band-type cavitation which fills the laminar separation bubble as shown in Figure 26 in the case of a circular cylinder which also exhibits a laminar separation bubble in the transcritical Reynolds number range.

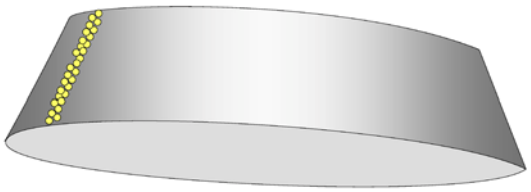

Figure 25: Schematic View of Cavitation Inception in a Laminar Separation Bubble at the Leading Edge of a Foil.

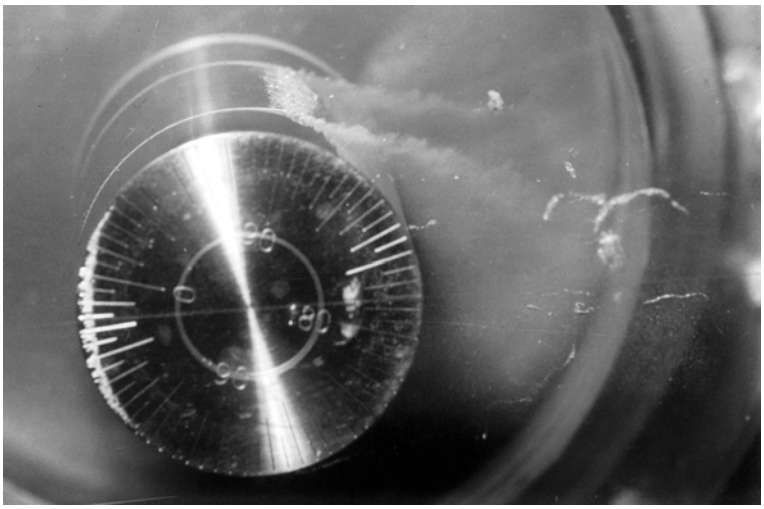

Figure 26: Band-Type Cavitation in the Laminar Separation Bubble on a Cylinder at a Transcritical Reynolds Number (Re = 290 000). A few vapour structures are also visible in the core of three dimensional streamwise vortices in the wake.

When the cavitation number is decreased, this band-type cavitation develops and forms a leading edge cavity as shown in Figure 5 whose length has nothing to do with the original length of the separation bubble.

A leading edge cavity is almost insensitive to water quality. The low pressure region which exists upstream cavity detachment is so short that the time available for bubble growth is very small. Nuclei cannot grow significantly upstream the cavity and thus do not affect this type of cavitation.

5.3 Case 3: Attached Turbulent Boundary Layer

For moderate values and usually in a quite limited range of angle of attack, another regime of boundary layer flow exists. The boundary layer does not separate at all, neither at the trailing edge nor at the leading

edge. This is illustrated by Figure 27 where turbulent spots, which are the signature of a transitional boundary layer, are visible.

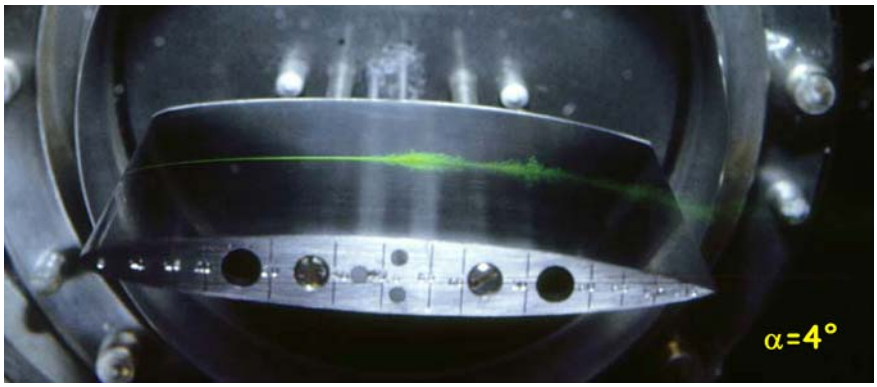

Figure 27: Attached Transitional Boundary Layer on a Hydrofoil.

The case of a fully attached turbulent boundary layer is also encountered on a cylinder at supercritical Reynolds number.

Since no separation exists, no attached cavity can exist neither. Cavitation generally appears in the form of spots attached to isolated roughness elements if any. It can also take the form of travelling bubbles originating from nuclei transported by the liquid.

We generally define the susceptibility pressure p_s of the liquid by the maximum critical pressure of the nuclei it contains. It is the critical pressure of the biggest nuclei (see section 2.3.2). Inception of travelling bubble cavitation occurs when the minimum pressure in the flow equals the susceptibility pressure. From a non-dimensional viewpoint, the minimum pressure coefficient at inception is given by:

$$\boxed{\sigma_i = -C_{p\,min} - \Delta\sigma} \tag{47}$$

where:

$$\boxed{\Delta\sigma = \frac{p_v - p_s}{\frac{1}{2}\rho V^2}} \tag{48}$$

The delay $\Delta\sigma$ in cavitation inception is connected to water quality. The closer the susceptibility pressure to the vapour pressure, the smaller the delay. On the other hand, the higher the flow velocity, the smaller the delay for a given water quality.

In some very special cases and particularly for very small values of the cavitation number and generally in a very limited range of incidence angle, a cavity can attach to the wall although the original boundary layer of the fully wetted flow does not separate. This seems to contradict the connection between separation and attached cavitation. Indeed, the existence of the cavity (which is largely developed at such a small cavitation number) significantly alters the pressure distribution on the wall in such a way that the boundary layer actually separates just upstream cavity detachment whereas no separation exists under fully-wetted flow conditions. This shows that, if a fully wetted flow analysis is satisfactory to account for cavitation inception, it may be insufficient in the case of developed cavitation because of the flow modifications due to cavitation itself.

6.0 PARTIAL CAVITATION

In this section devoted to partial cavitation, we will focus on the complex structure of the flow around cavity termination. A re-entrant jet develops which generally gives an unsteady behaviour to the cavity. The cloud cavitation instability, which is the most typical example of unsteady behaviour for a partial cavity, is described in detail.

6.1 Re-Entrant Jet and Cloud Cavitation Instability

The closure region of a cavity is the place where the flow reattaches to the wall. The liquid flow which goes along the cavity has locally the structure of a jet which impacts the wall. It splits in two parts. One is the re-entrant jet which travels upstream and brings a small quantity of water inside the cavity. The other one is the main outer flow which reattaches to the wall.

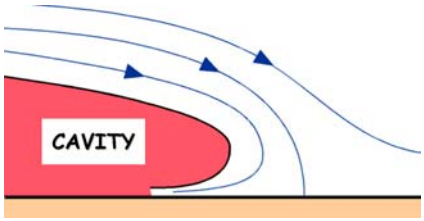

Figure 28: Schematic View of the Liquid Flow around Closure.

The existence of a re-entrant jet is unquestionable from a phenomenological viewpoint. The cavity is a region of minimum pressure so that the pressure gradient is everywhere directed away from the cavity. The streamlines close to the cavity are then forced to curve towards the cavity and a re-entrant jet automatically develops.

The re-entrant jet is separated from the outer flow by a streamline which, under steady conditions, would tend to end perpendicularly to the wall at a stagnation point. In practice, the situation is more fuzzy due to many factors and particularly unsteadiness and turbulence. Anyway, an overpressure actually exists near the cavity closure with a maximum pressure coefficient which generally does not exceed 0.2, a value which has to be compared to the $-\sigma_v$ value in the cavity.

It is clear that such a configuration cannot be steady unless the cavity would be progressively filled with liquid. A re-entrant jet actually exists only during part of the time. It progressively moves towards cavity detachment and when it comes into contact with the cavity interface, the cavity breaks up (see Figure 29). Its downstream part is entrained by the main flow and becomes a cloud of bubbles which will deform, gain some rotational movement before collapsing downstream. The upstream part, which may be quite small, remains attached to the wall and grows again into a new partial cavity which will give birth to a new re-entrant jet and the shedding of another cloud, and so on.

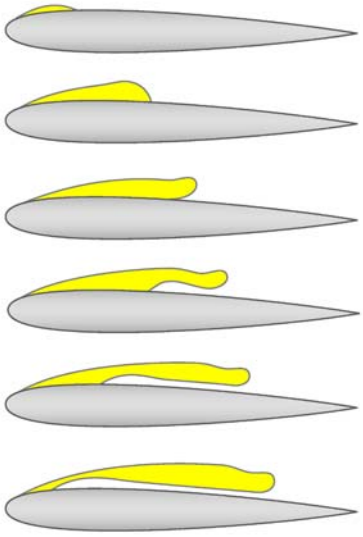

Figure 29: Development of a Re-Entrant Jet in the Closure Region of a Partial Cavity. The computation by BEM is stopped when the re-entrant jet hits the cavity interface (adapted from computations by De Lange & De Bruin, 1998).

In some cases, this behaviour is regular and periodic. This is the so-called cloud cavitation instability. The shedding frequency of clouds has been measured and also computed by numerous investigators. The corresponding Strouhal number is defined by:

$$S = \frac{f\,\ell}{V_\infty} \tag{49}$$

It is commonly based upon the maximum cavity length ℓ. Although a significant scattering exists mainly because of the difficulty to estimate cavity length, it is commonly agreed that the Strouhal number of the cloud cavitation instability lies between 0.25 and 0.4.

Figure 30 presents a typical visualization of the shedding of a cloud by a partial cavity. The importance of the re-entrant jet in the cloud cavitation instability has been proved by Kawanami et al. (1997). By putting a small obstacle on the wall inside the cavity, the re-entrant jet was stopped and the periodic shedding too.

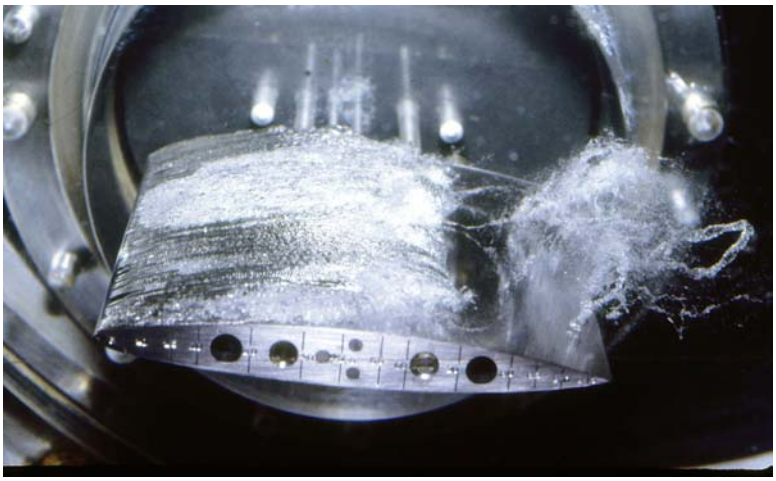

Figure 30: The Cloud Cavitation Instability and the Shedding of a Cloud by a Partial Cavity.

All partial cavities do not necessarily show the cloud cavitation instability. There are some factors which promote its development. In particular, the thickness of the cavity plays an important role. If the cavity is relatively thin, a strong interaction exists between the re-entrant jet and the cavity interface which results in the shedding of a large number of small scale vapour structures and not of a unique large scale cloud. The cloud cavitation instability is observed only for thick enough cavities (Callenaere et al. 1999).

Furthermore, the adverse pressure gradient is another factor which affects the cloud cavitation instability. A strong adverse pressure gradient will obviously increase the momentum of the re-entrant jet and so promote its upstream movement and the subsequent cloud cavitation instability.

In the case of a hydrofoil, the cloud cavitation instability is generally observed for cavity lengths around half the chordlength. Longer cavities close in regions of smaller adverse pressure gradient which is negative for the re-entrant jet. On the other hand, smaller cavities have a smaller thickness with also a negative consequence on the re-entrant jet as discussed above.

Although all partial cavities do not necessarily exhibit the cloud cavitation instability, the shedding of vapour structures is a permanent feature of all partial cavities. There is a great variety in size and shedding frequency of the vapour structures produced by partial cavities and the shedding process often appears as confused and chaotic. Cloud cavitation is the most regular and coherent regime of oscillation of partial cavities.

6.2 Three-Dimensional Effects

The closure region of partial cavities can be affected by three-dimensional effects although the geometry of the foil remains two-dimensional. In the case of Figure 30, two-dimensionality prevails. The closure line is perpendicular to the main flow velocity and a unique cloud is shed all along the foil span.

Conversely, three-dimensional effects are clearly visible for the partial cavity of Figure 31. The closure line is irregular. Two clouds are shed along the span and there is a lack of coherence between the two sheddings.

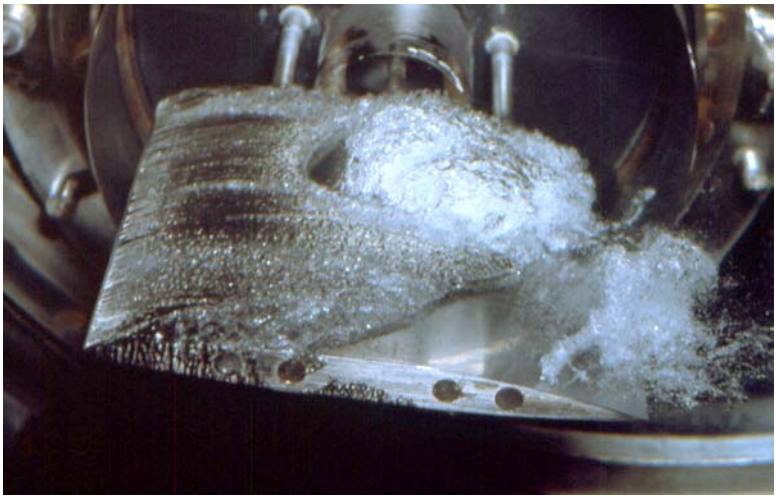

Figure 31: Three-Dimensional Effects at Cavity Closure.

Kawanami et al. (1998) have shown that the coherence of the shedding process decreases when the span length increases in comparison to the cavity length. The phenomenon has been investigated experimentally for a hydrofoil of given span length. They measured the spanwise length of the vapour structures shed by partial cavities for different cavity lengths. They showed that the spanwise length is of the order of the

streamwise cavity length. When the cavity length is decreased, the spanwise length of the vapour structures is also decreased, so that there is a larger number of structures shed along the span.

They identified several regimes. The regime with a unique shedding all along the span corresponds to the cloud cavitation instability mentioned above. Other regimes with the shedding of two or three clouds were observed for smaller cavities. An irregular beak-off mechanism was also observed when there is no matching between the shedding process and the foil span.

Three dimensional effects also appear in the case of swept hydrofoils. Such a configuration was investigated by Laberteaux and Ceccio (2001). An important feature is the direction of the re-entrant jet. In the case of an inclined cavity closure line, De Lange and De Bruin (1998) have shown that the re-entrant jet is no longer travelling counter current but is deviated and gains a spanwise component which affects the cavity break-off mechanism.

REFERENCES

Brennen C.E. (1994) "Hydrodynamics of pumps" *Concepts ETI Inc. & Oxford University Press*.

Brennen C.E. (1995) "Cavitation and Bubble Dynamics" *Oxford University Press*.

Callenaere M., Franc J.P. & Michel J.M. (2001) "The cavitation instability induced by the development of a re-entrant jet" *J. Fluid Mech.*, **444**, 223-256.

De Lange D.F. & De Bruin G.J. (1998) "Sheet cavitation and cloud cavitation, re-entrant jet and three-dimensionality" *Appl. Sci. Res.* **58**, 91-114.

Franc J.P. and Michel J.M. (2004) "Fundamentals of cavitation" *Kluwer*.

Fruman D.H., Reboud J.L. & Stutz B. (1999) "Estimation of thermal effects in cavitation of thermosensible liquids" *Int. J. of Heat and Mass Transfer*, **42**, 3195-3204.

Fujikawa S. & Akamatsu T. (1980) "Effects of non-equilibrium condensation of vapor on the pressure wave produced by the collapse of a bubble in a liquid" *J. Fluid Mech.*, **97**, Part 3, 481-512.

Holl J.W., Billet M.L. & Weir D.S. (1975) "Thermodynamic effects on developed cavitation" *J. of Fluids Eng.*, Dec.1975, 507-514.

Kato H. (1984) "Thermodynamic effect on incipient and developed sheet cavitation" *Proc. Int. Symp. on Cavitation inception, FED-Vol.16*, New-Orleans (USA), Dec. 9-14, 1984, 127-136.

Kawanami Y., Kato H. & Yamaguchi H. (1998) "Three-dimensional characteristics of the cavities formed on a two-dimensional hydrofoil" *Proc. 3rd Int. Symp. on Cavitation*, Grenoble, France, **Vol. 1**, 191-196.

Kawanami Y., Kato H., Yamaguchi H., Tagaya Y. & Tanimura M. (1997) "Mechanism and control of cloud cavitation" *J. Fluids Eng.*, **119**, 788-795.

Laberteaux K. & Ceccio S.L. (2001) "Partial cavity flows. Part 1 – Cavities forming on models without spanwise variation. Part 2 – Cavities forming on test objects with spanwise variation" *J. Fluid Mech.*, **431**, 1-41 and 43-63.

Stepanoff A.J. (1964) "Cavitation properties of liquids" *J. of Eng. for Power*, April 1964, 195-200.

Watanabe S., Hidaka T., Horiguchi H., Furukawa A. & Tsujimoto Y. (2005) "Steady analysis of thermodynamic effect of partial cavitation using singularity method" *Proc. of FEDSM2005*, June 19-23, Houston, USA.